

LS-115
W. Chou and Y. Jin
July 1988

**IMPEDANCE STUDIES - PART 4:
THE APS IMPEDANCE BUDGET**

This note will wrap up the numerical results that were obtained in our calculations of the wake potentials, the loss factors, and the impedances for a variety of structures in the APS storage ring. It consists of five sections and one appendix. Section 1 is an introduction. Section 2 summarizes the hand calculations. The computer calculations are the subject of Section 3. Section 4 discusses several tests in our numerical methods. Section 5 presents the APS impedance budget, along with some discussion. The appendix contains the figures of the structures, the longitudinal/transverse wake potentials and the real/imaginary part of the impedances of various sorts of geometries that have been included in the budget.

1. INTRODUCTION

The APS impedance budget is a product of several different sorts of work. One is the hand calculations, which employ existing formulae to estimate the impedances of some simple cases, such as free space, space charge, resistive wall and beam position monitors (BPMs). For other cases, especially those which involve complex geometries, one has to invoke numerical calculations. The 2D code TBCI is used to study 2D geometries, such as the RF cavities. For more complicated structures, e.g. the beam chamber and the antechamber, the crotch absorbers, the bellows, the valves, the scrapers and the transitions between vacuum chambers with different transverse dimensions, etc., we use the 3D code MAFIA. Either TBCI or MAFIA computes wake potentials, which are then transformed to impedances through an FFT program. Certain parts of the APS facility, including the injection and abort sections and many diagnostic instruments, have not yet been designed in full detail. The loss factors of these parts are estimated by using the PEP-measured data sheet (Ref. 1).

2. HAND CALCULATIONS

A. The Cutoff Frequency of an Elliptical Beam Chamber

The cutoff frequency of a beam chamber can be calculated analytically when the cross-section is an ellipse (Ref. 2). Figure 1 shows the wavelengths of several lower order modes of an elliptical pipe as functions of the eccentricity. The vacuum chambers used in the APS storage ring have basically two different sizes. Their cutoff frequencies of the TM01 wave and the corresponding mode numbers are listed in Table 1.

Table 1

	major axis (cm)	minor axis (cm)	eccentricity	$f_{cut}(\text{TM01})$ (GHz)	n_{cut}^*
Beam Chamber	8.47	4.17	0.87	4.6	1.6×10^4
ID Section	5	0.8	0.987	16	5.7×10^4

* $n_{cut} = f_{cut}/f_o$, in which $f_o = 0.2828$ MHz is the revolution frequency.

B. Free-Space Impedance

The synchrotron radiation contributes to the coupling impedance through the Bonch-Osmolovsky formula:

$$\frac{Z_{\parallel}}{n} = 0, \quad n < n_{cut}$$

$$= \frac{354}{273} \left(\frac{\rho}{R} \right)^{1/3} \left(\frac{\sqrt{3} + i}{2} \right), \quad n_{cut} \leq n < n_{crit}$$

and

$$Z_{\perp} = 0,$$

in which ρ is the bending radius, R the averaged machine radius, n_{cut} the mode number at the cutoff and n_{crit} that at the critical frequency of the synchrotron radiation. Using $\rho = 38.96$ m, $R=168.7$ m, we get

$$\left| \frac{Z_{\parallel}}{n} \right| = 0.34 \Omega, \text{ for } n = n_{cut}.$$

C. Space-Charge Impedance

For a circular cross-sectional beam with radius b traversing a circular cross-sectional beam chamber with radius r , the coupling impedances due to space charges are given by

$$\frac{Z_{\parallel}}{n} = -i \frac{Z_0}{2\beta\gamma^2} \left(1 + 2 \ln \frac{r}{b} \right)$$

and

$$Z_{\perp} = -i \frac{RZ_0}{\beta^2\gamma^2} \left(\frac{1}{b^2} - \frac{1}{r^2} \right).$$

Because both the longitudinal and the transverse impedances are proportional to the inverse square of the particle energy γ , we expect that they would be insignificant at 7 GeV. This means that one may use some equivalent radii for the elliptical beam and the elliptical beam chamber of the APS storage ring in these formulae to get a rough estimation. The results are

$$\left| \frac{Z_{\parallel}}{n} \right| = 1 \times 10^{-5} \Omega, \text{ at } n = n_{cut}$$

and

$$|Z_{\perp}| = 0.032 \text{ M}\Omega/\text{m}.$$

D. Resistive-Wall Impedance

For a beam chamber with a circular cross-section of radius r and a wall resistivity ρ_w , the resistive-wall impedance can be easily calculated.

$$\frac{Z_{\parallel}}{n} = \frac{1+i}{n} \left(\frac{Z_0 R \rho_w}{2r^2} \right)^{1/2},$$

and

$$Z_{\perp} = \frac{2R}{r^2} \frac{Z_{\parallel}}{n}.$$

For the APS, we have

$$\left| \frac{Z_{\parallel}}{n} \right| = 0.014 \Omega, \text{ at } n = n_{\text{cut}}$$

$$|Z_{\perp}| = 0.013 \text{ M}\Omega/\text{m}.$$

For a beam chamber with a rectangular cross-section, the corresponding formulae have been derived in Ref. 3. It is shown that when the displacement of the beam from the center is small, the results are smaller than those for a circular one. It is reasonable to assume that the impedances of an elliptical beampipe should be between the two cases. Therefore, it is safe to use the above values in our estimation.

E. Impedances of BPMs

The BPMs used in the APS storage ring are of four-button type, see Fig. 2. The formula to calculate their impedances can be found in Ref. 4.

$$\frac{Z_{\parallel}}{n} = i 2\pi Z_c \frac{4d}{2\pi R} \left(\frac{\phi_o}{\pi} \right)^2, \text{ for } f < \frac{c}{2d}$$

$$= \frac{1}{n} \frac{Z_c^2}{Z_T} \left(\frac{\phi_o}{\pi} \right)^2, \text{ for } f = \frac{c}{2d} (2k-1)$$

in which Z_c is the characteristic impedance, Z_T the termination impedance, ϕ_o/π the effective semi-angular aperture and d the diameter of the button. For a total number of 360 BPMs, we get

$$\left| \frac{Z_{\parallel}}{n} \right| \leq 0.02 \Omega.$$

3. COMPUTER CALCULATIONS

The 3D MAFIA and the 2D TBCI are employed to compute the wake potentials generated by a Gaussian-distributed rigid bunch passing through

various geometries. Because 3D codes consume enormous memory space and CPU time, one should be careful in designing a mesh. MAFIA allows for a non-uniform grid. That greatly increases the flexibility. (But note that the grid size in the bunch moving direction has to be uniform.) When a structure possesses certain symmetry, one may make use of it to reduce the number of mesh points. For example, for a geometry with an elliptical cross-section, only one-fourth of the structure is needed in calculating the longitudinal wake and one-half in computing the transverse wakes. The CPU time is approximately linearly proportional to the product of the total mesh points and the total time steps. It is about 0.03 ms per mesh point per time step on a VAX 8700, provided that the working set size can be as big as the program requires. Otherwise, the CPU time could be increased dramatically due to page faults. Some geometries (e.g. scraper) call for the so-called direct method in wake potential integration, which is slower than the indirect method.

The rms bunch length, σ_b , is set to 1.75 cm in the calculations. This corresponds to a bunch lengthening factor of 3. The mesh size along the bunch moving direction is chosen as $dz = 0.35$ cm in MAFIA. This choice is a compromise between MAFIA and FFT. On the one hand, MAFIA requires that the ratio σ_b/dz should be 5 or greater in order to keep the accuracy of the results. On the other hand, however, if this ratio is too large, a lot of information will be lost when one converts the impedance for a bunch to that for a point charge. This will be explained later.

An average MAFIA job uses about 60,000 mesh points, 8 MB virtual memory. The CPU time on a VAX 8700 is about 5 hours to get 512 data points for wake potentials, which will then be used in FFT. In certain cases, only the loss factors are of interest, and the number of wake points to calculate can be much less (50 or so).

The RF cavities have a rotational symmetry which makes 2D computation possible. In this case, we first use TBCI to get the total loss factor, from which the loss factor of the fundamental mode (i.e., TM01), obtained from URMEL, is then subtracted. The wake calculations are similar to those in the 3D case, except that one has to use a uniform grid in TBCI.

There are several things that should be pointed out about the Fourier transform. Assume that the Gaussian-distributed bunch has an rms

length σ_b and that the calculated wake potentials are $W_{||}(m)$, $m=0, 1, \dots, n-1$, where n is the total number of data, with $W_{||}(0)$ being the wake at the center of the bunch. (The reader is referred to Ref. 5 for this little trick.) Then the longitudinal impedance for the bunch is defined by

$$\tilde{Z}_{||}(k) = -dt \sum_{m=0}^{n-1} W_{||}(m) \cdot \exp(-2\pi imk/n), \quad k=0, 1, \dots, n-1$$

in which dt is the time step ($dt=dz/c$). The minus sign on the righthand side reflects the fact that the distance behind the first particle of the bunch is taken to be negative. A similar definition holds for the transverse impedance, except that one multiplies on the righthand side by a $(-i)$. The Nyquist critical frequency is given by

$$f_c = \frac{1}{2 dt},$$

which determines the band-width of the impedance. The resolution of FFT is

$$\Delta f = \frac{2f_c}{n}$$

$$= \frac{1}{n dt}.$$

However, when one converts the impedance for a Gaussian bunch, $\tilde{Z}(k)$, to that for a point charge, $Z(k)$, through the formula

$$Z(k) = \tilde{Z}(k) \exp\left[\frac{1}{2}\left(\frac{2\pi k \cdot \Delta f \cdot \sigma_b}{c}\right)^2\right], \quad k = 0, 1, \dots, n-1$$

the useful band-width will be much smaller than f_c . This is because the exponential factor on the righthand side would wash out any useful information contained in $\tilde{Z}(k)$ when k is close to n . For instance, at the Nyquist frequency, one would have

$$Z = \tilde{Z} \exp\left[\frac{\pi^2}{2}\left(\frac{\sigma_b}{dz}\right)^2\right],$$

and the ratio σ_b/dz is usually 4 or 5 or even larger! Therefore, we take the useful frequency region to be

$$f \leq f_{\max} = \frac{f_c}{\sigma_b / dz}$$

$$= \frac{c}{2 \sigma_b} .$$

Then, at $f = f_{\max}$, one would have

$$z \sim 140 \tilde{z} .$$

It is obvious that this useful frequency region depends only on the bunch length. In most of our calculations, we have

$$\sigma_b = 1.75 \text{ cm},$$

$$dz = 0.35 \text{ cm},$$

$$\sigma_b / dz = 5,$$

$$n = 512,$$

$$dt = 1.2 \times 10^{-11} \text{ s},$$

$$f_c = 43 \text{ GHz},$$

$$f_{\max} = 8.6 \text{ GHz}$$

$$\Delta f = 0.17 \text{ GHz}.$$

For bellows and valves, dz is 0.175 cm.

4. TESTING THE NUMERICAL METHODS

There are several simple geometries whose impedances have been derived analytically (Ref. 6 and 7). These known results provide us with an ideal way to check our numerical method. (Another way is to compare the numerical results with real measurements. This type of work is in progress.) We choose the two geometries discussed in Ref. 7 for testing (see Fig. 3). They are called the expansion and the pinch component, respectively, in a previous note (Ref. 8). These seemingly simple geometries involve fairly complicated calculations due to the fact that the entrance and the exit beampipes have different radii. We use TBCI to compute the longitudinal wake potential by integrating the electric field on the axis, keeping an eye on the effects of the truncated length L_{in} and L_{out} (Ref. 8). Once the output of the

integration becomes stable, another integrated value obtained from a second run (which assumes a smooth-pipe geometry) is subtracted from it. The difference gives the corrected wake potential and is shown in Fig. 4. The impedances can then be readily obtained from FFT, as shown in Fig. 5. The calculated results of the impedances in Ref. 7 are reproduced in Fig. 6, with the horizontal axis being rescaled. Comparing Fig. 5 with Fig. 6, it is seen that the zero-frequency impedance (i.e., the averaged wake) and the locations of the first few resonant peaks agree with each other fairly well. The amplitudes of the peaks calculated by TBCI and FFT are larger than those in Ref. 7, probably due to the limited number of terms included in a series expansion in Ref. 7, but this has not been verified. The first peak of $\text{Re } Z$ in Fig. 5 is split into two, a phenomenon that has not yet been understood.

In another test, we took the bellows structure studied by the SSC group (Ref. 5) and reproduced the results of their impedance calculations.

The comparison between MAFIA and TBCI is under way. The preliminary results are a bit confusing. While both programs gave almost the identical loss factors in two tests, in a third run the results from the two codes differed by 50%. The reason is still unknown.

5. APS IMPEDANCE BUDGET

The results of our impedance calculations are summarized in Table 2. Some longitudinal loss factors are obtained from PEP measurements. The impedance for a bunch and for a point charge are listed in separate columns. The mode number n in Z_{\parallel}/n is that at the cutoff frequency of the beam chamber, namely, 1.6×10^4 .

All the impedance values listed in Table 2 have been multiplied by the number of structures. For RF cavities, the contribution of the fundamental mode has been subtracted from the results.

It is seen clearly that the largest longitudinal loss is contributed by the RF cavities, whereas the largest transverse loss is contributed by the transitions between the beam chamber and the ID section. It can be shown that the vertical dimension of the ID section is the most critical parameter as far as the single bunch current limit is concerned. As a matter of fact, the vertical loss factor would be reduced to half of its listed value if the

vertical loss factor would be reduced to half of its listed value if the vertical size of the ID section was increased from 8 mm to 12 mm. Other possible approaches to reducing the transverse impedances would include, for example, a careful design of the tapered part in the transitions.

Table 2. APS Impedance Budget (bunch length = 1.75 cm)

Structure	Number	Loss Factor		Z For a Bunch		Z For a Point Charge	
		$k(z)$ (V/pC)	$k(x)$ (V/pC/m)	$k(y)$ (V/pC/m)	$Z(z)/n$ (Ohm)	$Z(x)$ (Mohm/m)	$Z(y)$ (Mohm/m)
A. Vacuum Chamber:							
1. Transition between cham w & w/o ante	3 x 40	1E-6	0.4	-0.07	5.3E-5	1E-4	2.4E-5
2. Transition between chamber & ID	34	0.068	-75	1160*	0.03	7.5E-3	0.027*
3. Transition between chamber & RF	3	0.057	-0.3	57	7.5E-3	4.2E-3	6.75E-3
4. Crotch absorber	2 x 40	1E-5	0.6	-0.1	2.5E-5	8E-5	1.6E-5
5. Bellows (shielded)	6 x 40	0.06	29	110	0.018	4E-3	7.2E-3
6. Valve	2 x 40	0.001	11	16	6.5E-4	3E-3	2.4E-3
7. Lumped ion/neg pump port (screened)	5 x 40	0.6					
B. RF Cavities: (HOM)							
1. 353 MHz	15	2.9	34	34	0.16	0.023	0.023
2. 1059 MHz	10						
C. Diagnostics:							
1. BPM	9 x 40						
2. Beam scraper	2						
3. Current transformer	2						
4. Horz hf pickup electrode	2						
5. Vert hf pickup electrode	2						
6. Horz pinger	2						
7. Vert pinger	2						
D. Injection & Abort Sections:							
1. Injection bumper	4						
2. Abort kicker	2						
3. Injec thin pulsed septum	1						
4. Lambertson septum	1						
5. Injec Y beamport & cham	1						
6. Extrac Y beamport & cham	1						
E. Other Sources:							
1. Synch. radiation							
2. Space charge							
3. Resistive wall							
F. Ignored:							
1. Bent chamber in dipoles							
2. Photon beam port							
3. Injec thin dc septum	1						
4. Injec thick dc septum	1						
G. Unused budget reserved for unforeseen parts:							
1.5	182	495	0.66	0.05	0.21	0.8	0.14
TOTAL	6.2	180	1900	0.9	0.1	0.3	2
						0.4	0.7

10

* These numbers are obtained from TBCI. The MAFIA output for these parameters are under testing.

REFERENCES

1. J. N. Weaver, P. B. Wilson, and J. B. Styles, IEEE Trans. Nucl. Sci., NS-26, 3971 (1979).
2. L. J. Chu, J. Appl. Phys., V.9, p. 583 (1938).
3. K. Y. Ng, Particle Accelerators, V.16, p. 63 (1984).
4. A. G. Ruggiero, Proc. 1979 Workshop on Beam Current Limitations in Storage Rings, BNL, July 16-27, 1979, p. 47.
5. K. Y. Ng, SSC-SR-1017, p. 47 (1985).
6. H. Henke, CERN-LEP-RF/85-41 (1985).
7. S. A. Kheifets and S. A. Heifets, Proc. 1986 Linear Accelerator Conference, Stanford, California, SLAC-303, p. 493.
8. W. Chou and Y. Jin, "Impedance Studies-Part 1: A Composition Rule," ANL Light Source Note LS-112 (1988).

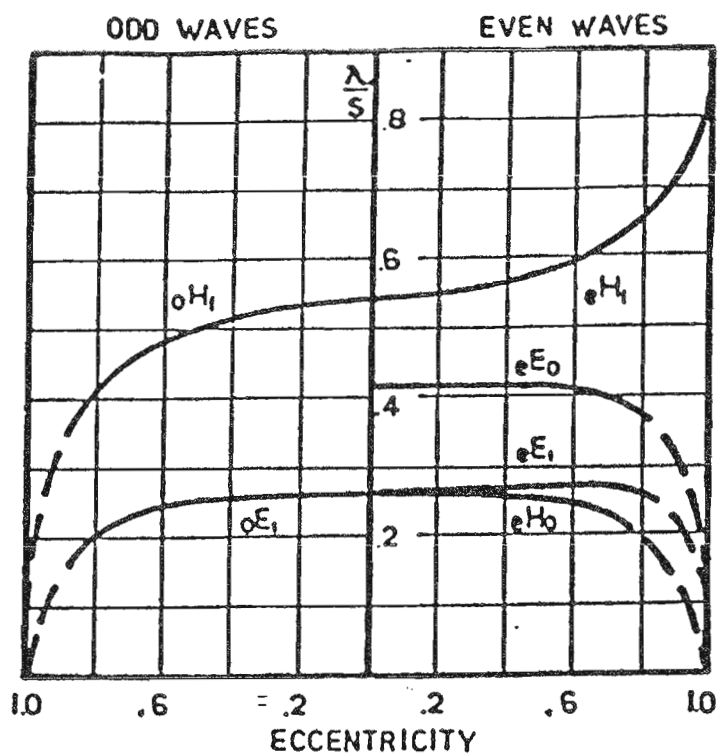


Fig. 1. Critical wavelength of waves in an elliptical pipe, with s the periphery of the pipe.

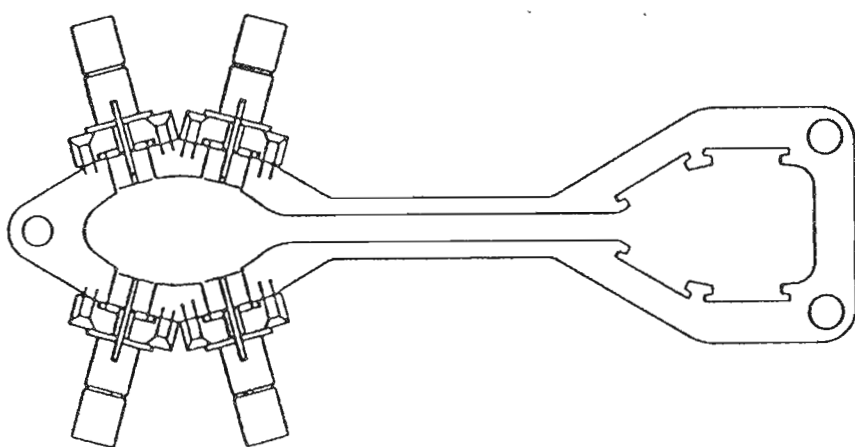
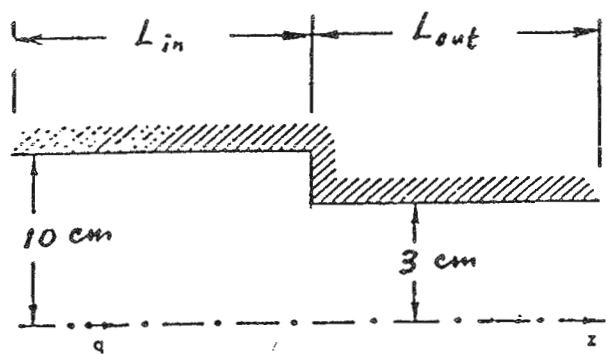
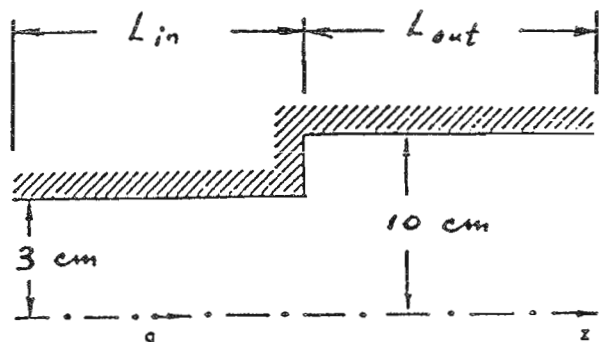


Fig. 2. Vacuum chamber cross section showing beam position monitor assembly.

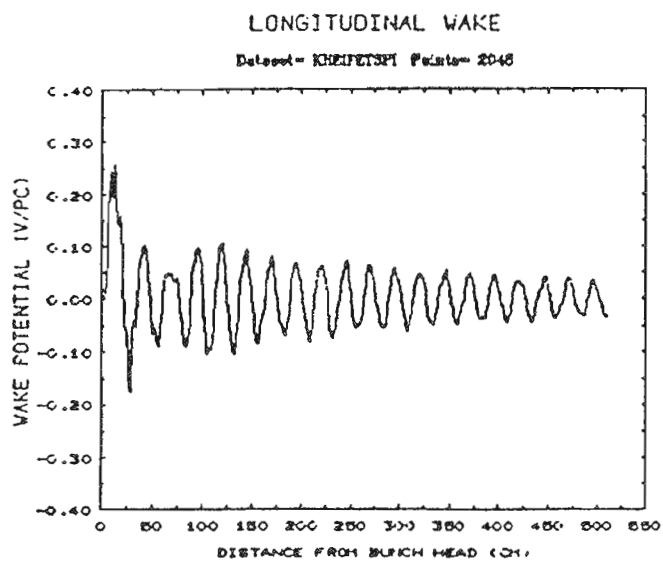


(a)

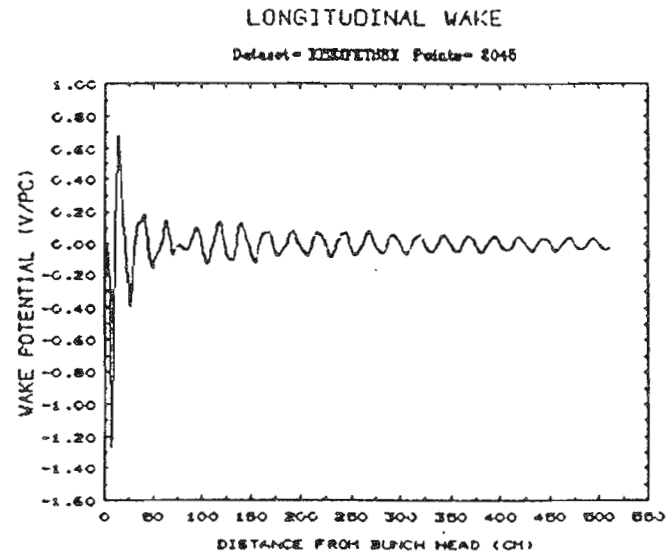


(b)

Fig. 3. (a) Pinch and (b) expansion geometries used in testing.

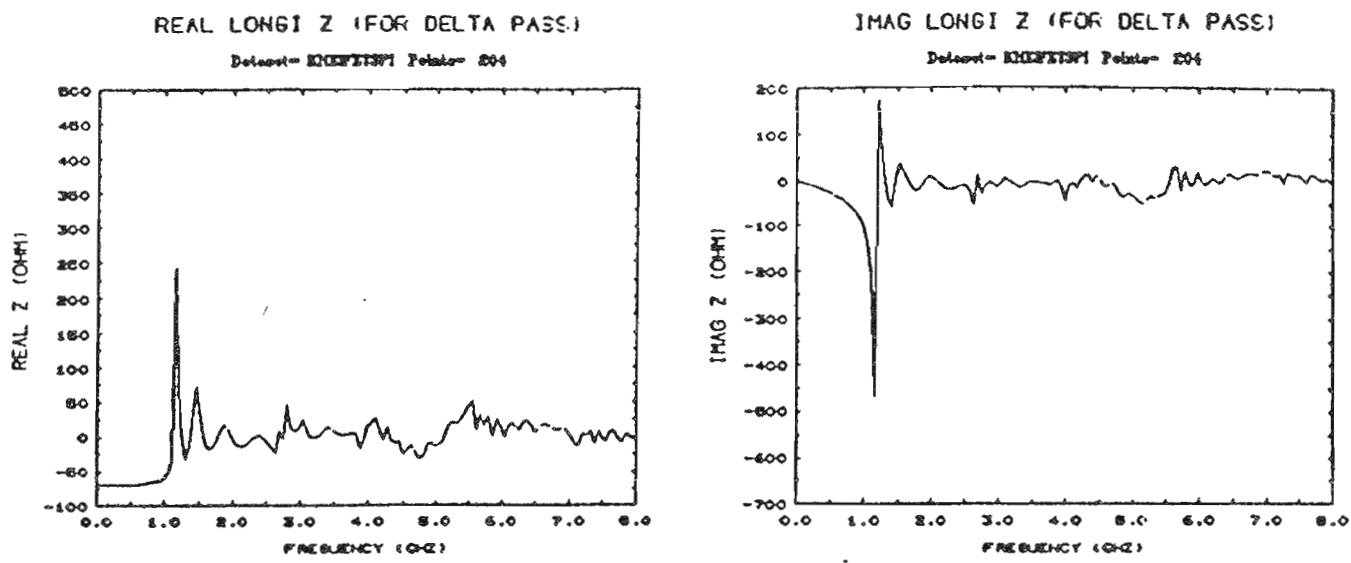


(a)

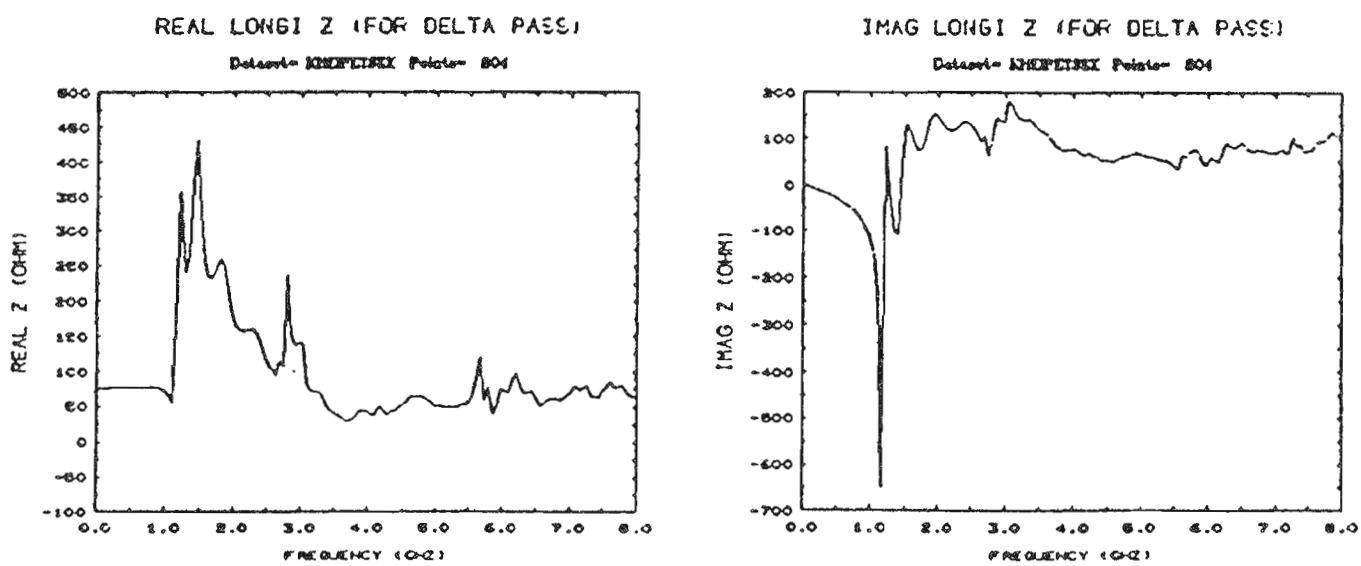


(b)

Fig. 4. Longitudinal wake potentials obtained from TBCI for (a) pinch and (b) expansion.



(a)



(b)

Fig. 5. Real and imaging parts of impedances obtained from FFT for (a) pinch and (b) expansion.

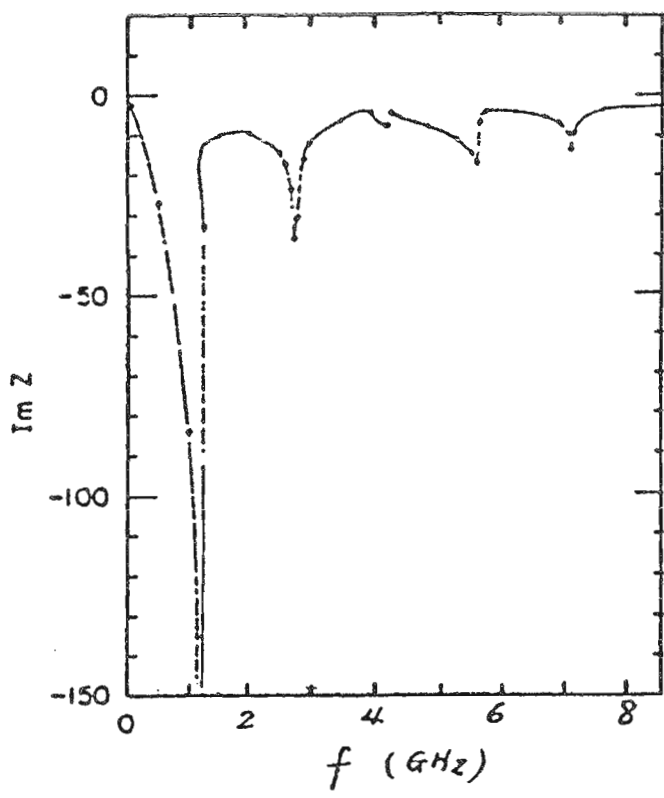
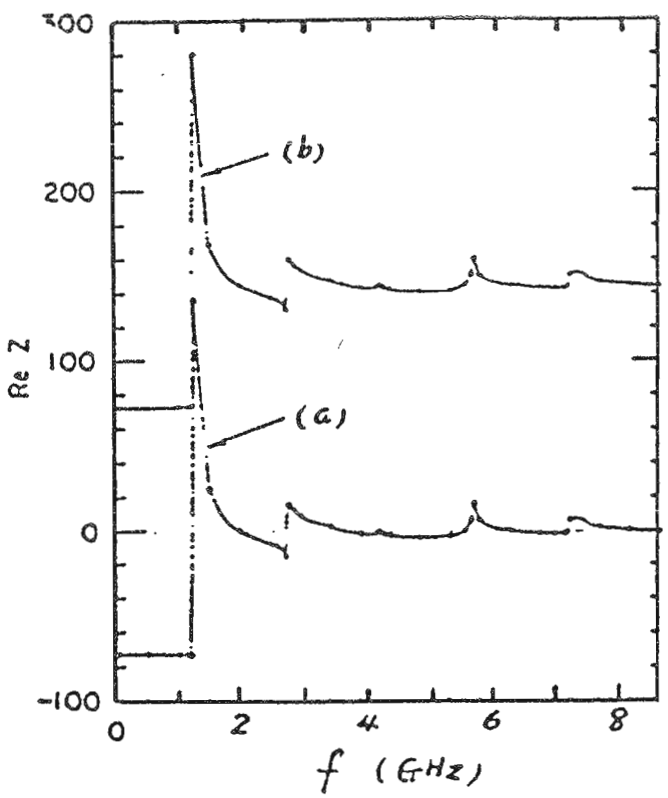


Fig. 6. Real and imaginary parts of impedances calculated in Ref. 7 for (a) pinch and (b) expansion. The horizontal axis has been rescaled.

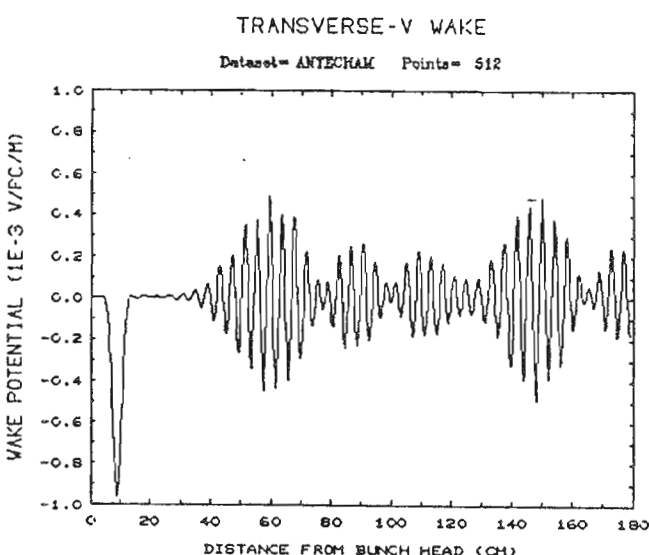
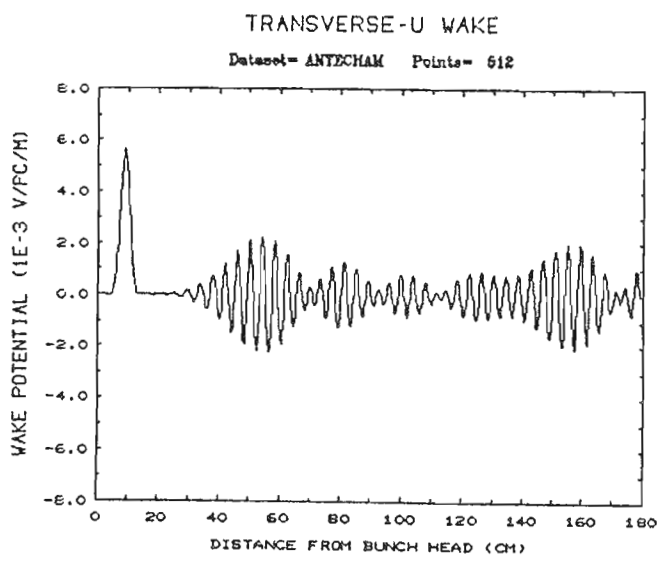
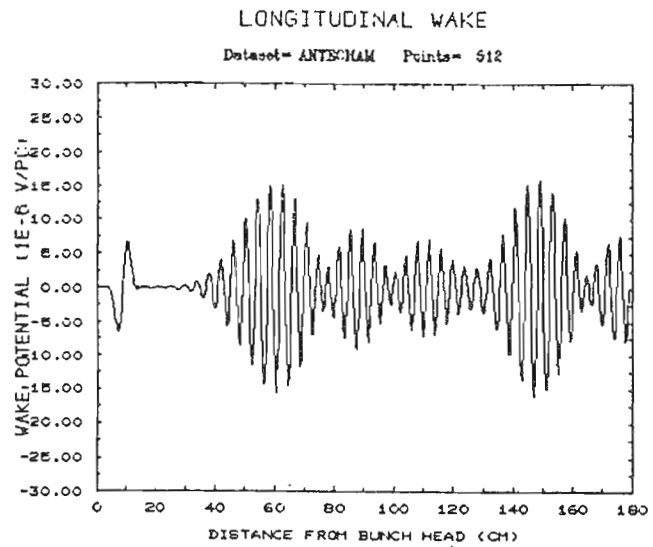
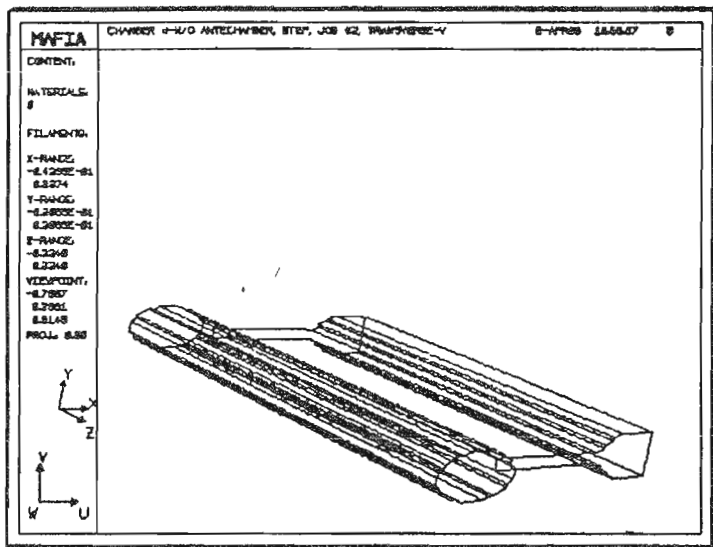
Appendix to LS-115

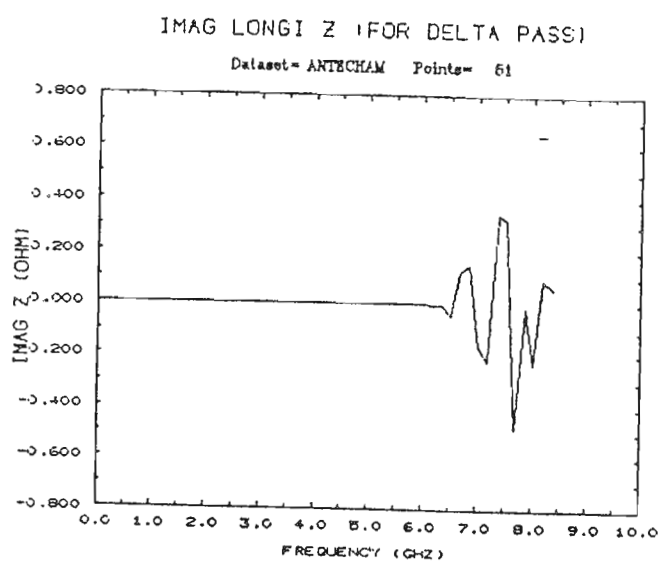
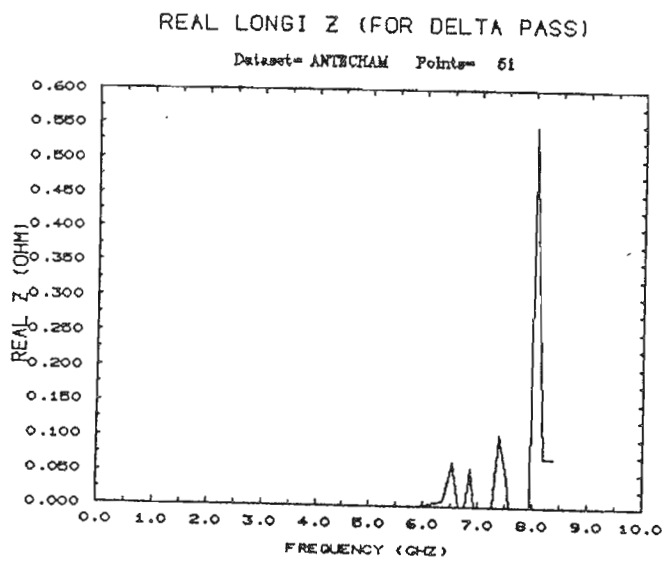
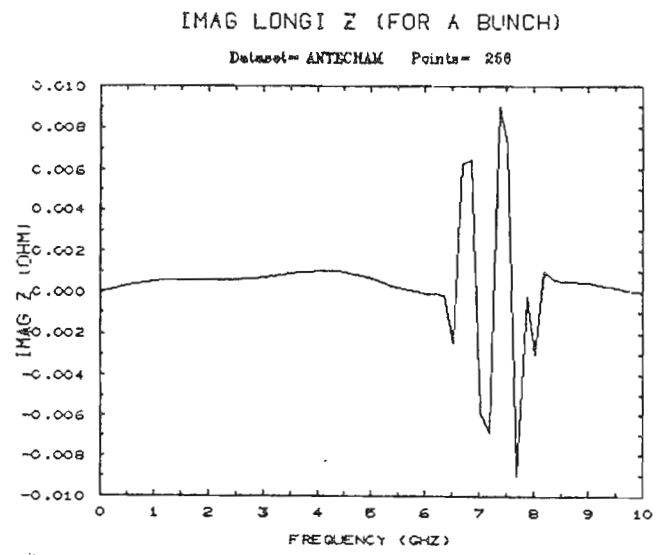
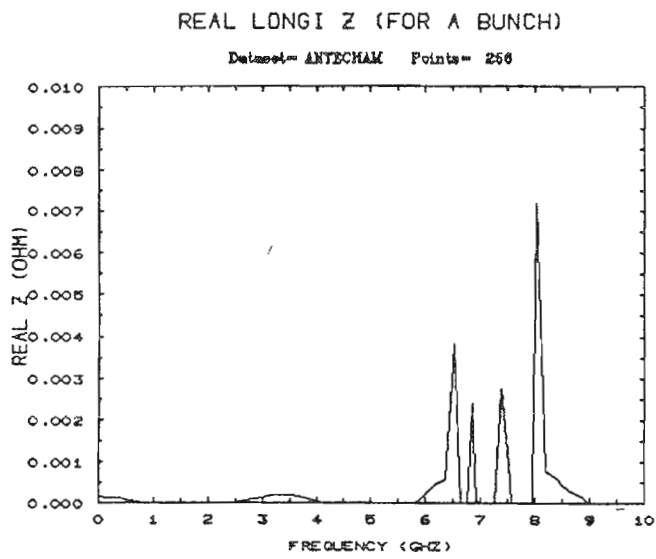
The figures in the computer calculations for the impedances of the APS storage ring are presented in this appendix. For each structure, we show (a) the geometry used in our calculations, (b) the longitudinal, the transverse-U (i.e., horizontal), and the transverse-V (i.e., vertical) wake potentials, (c) the real/imaginary part of the impedance seen by a bunch in each direction, and (d) the real/imaginary part of the impedance seen by a point charge in each direction.

The following is a list of structures included in this appendix:

1. transition between beam chambers with and without antechamber,
2. transition between beam chamber and insertion device (ID) section,
3. transition between beam chamber and RF section,
4. crotch absorber,
5. bellows (shielded),
6. valve,
7. RF cavity (353 MHz),
8. third harmonic RF cavity (1059 MHz),
9. beam scraper.

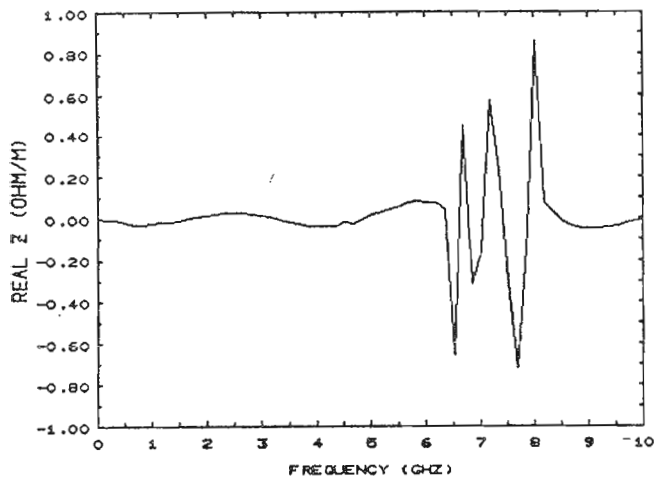
1. TRANSITION BETWEEN BEAM CHAMBERS WITH AND WITHOUT ANTECHAMBER.





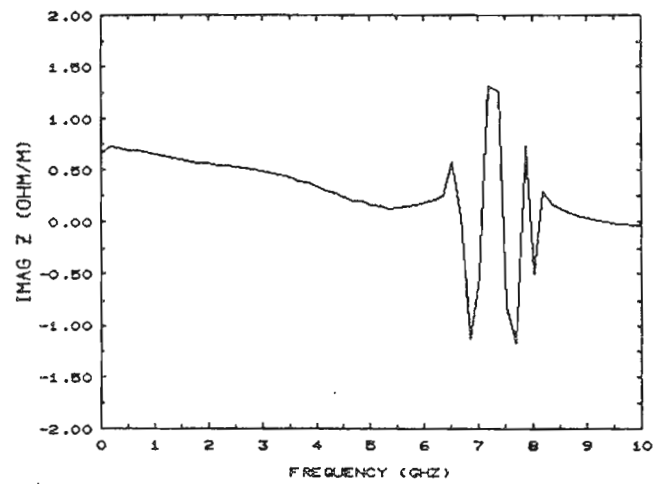
REAL TRANS-U Z (FOR A BUNCH)

Dataset= ANTECHAM Points= 256



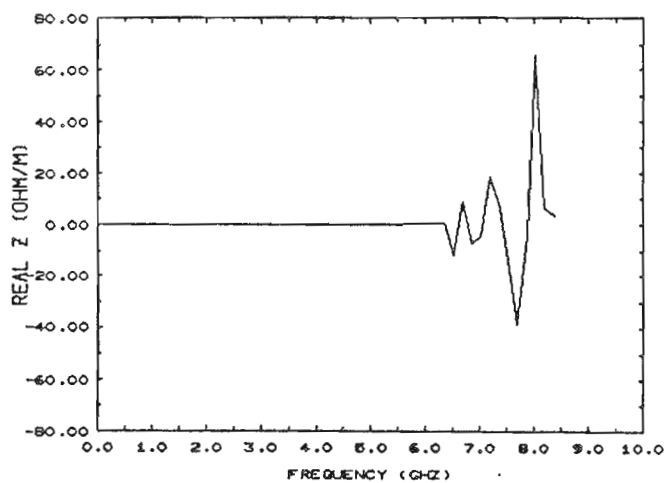
IMAG TRANS-U Z (FOR A BUNCH)

Dataset= ANTECHAM Points= 256



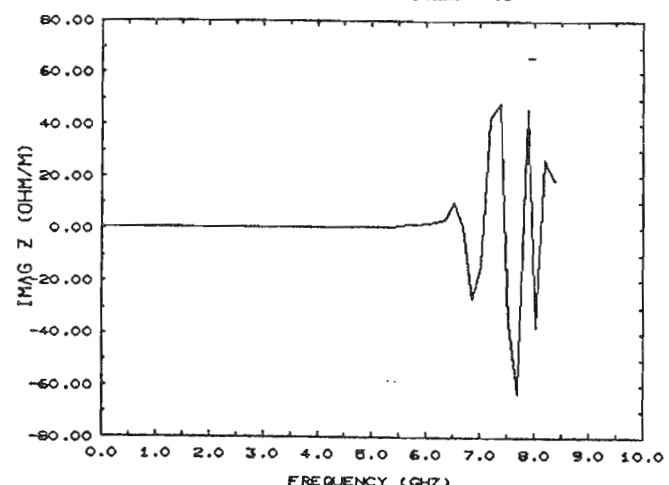
REAL TRANS-U Z (FOR DELTA PASS)

Dataset= ANTECHAM Points= 51



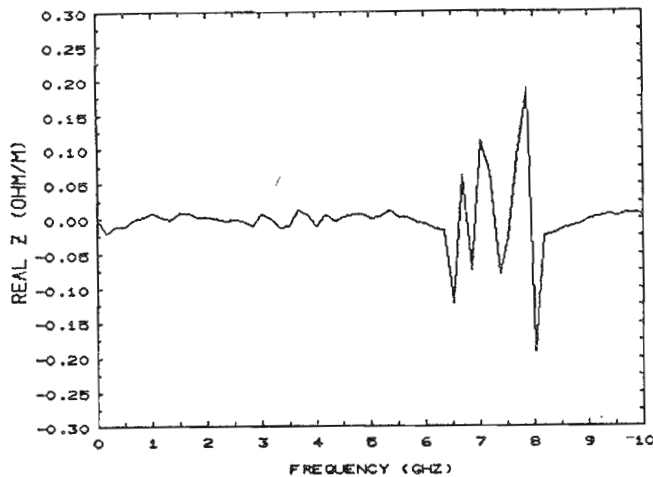
IMAG TRANS-U Z (FOR DELTA PASS)

Dataset= ANTECHAM Points= 51



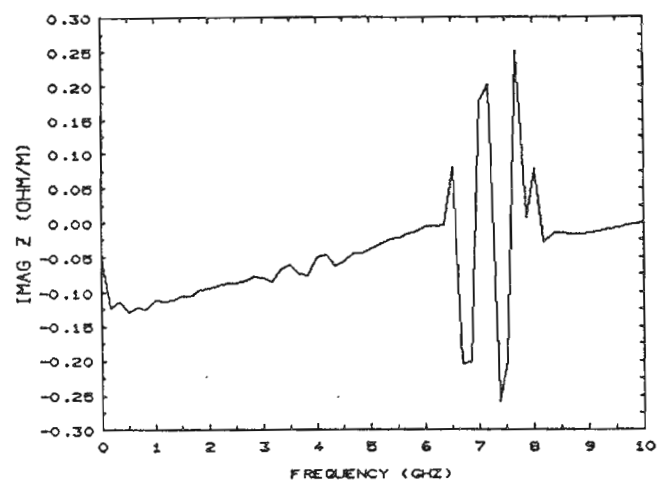
REAL TRANS-V Z (FOR A BUNCH)

Dataset= ANTECHAM Points= 256



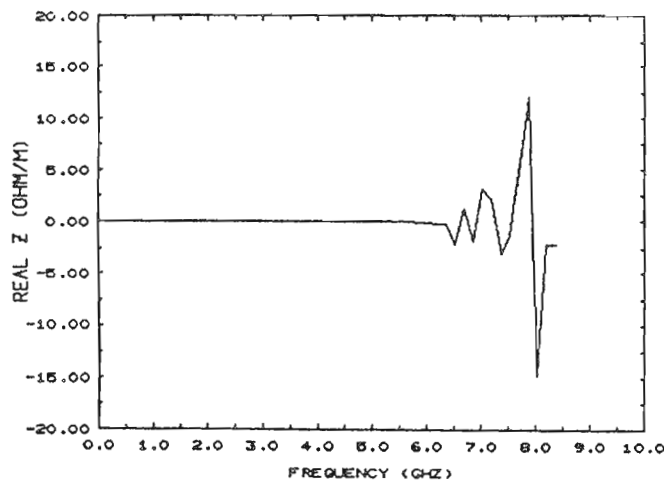
IMAG TRANS-V Z (FOR A BUNCH)

Dataset= ANTECHAM Points= 256



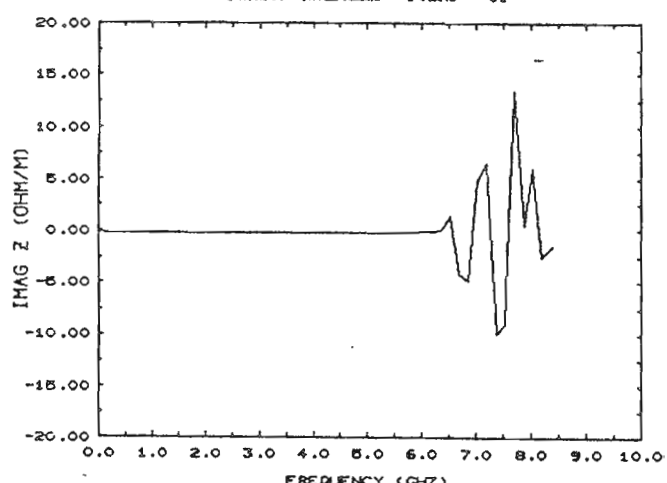
REAL TRANS-V Z (FOR DELTA PASS)

Dataset= ANTECHAM Points= 61

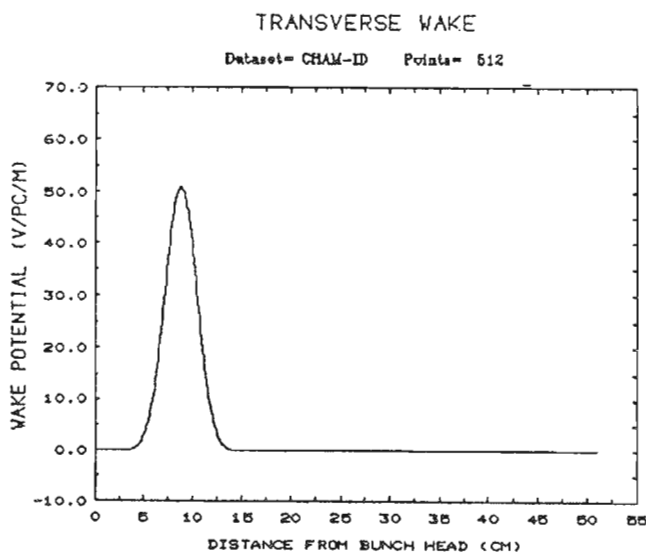
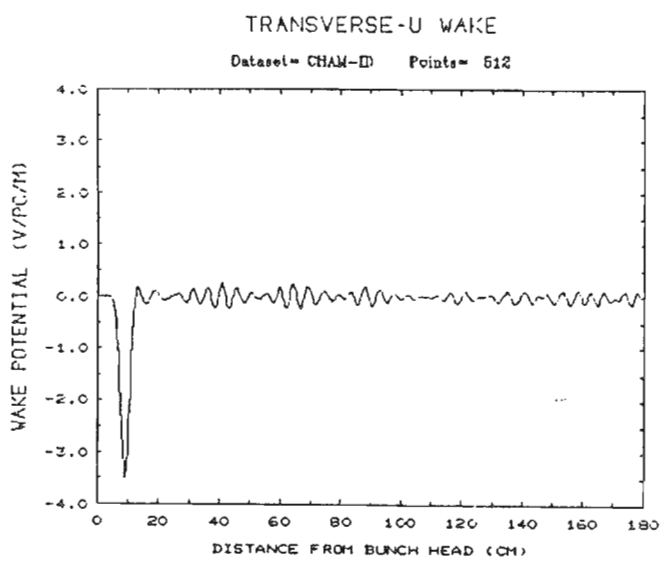
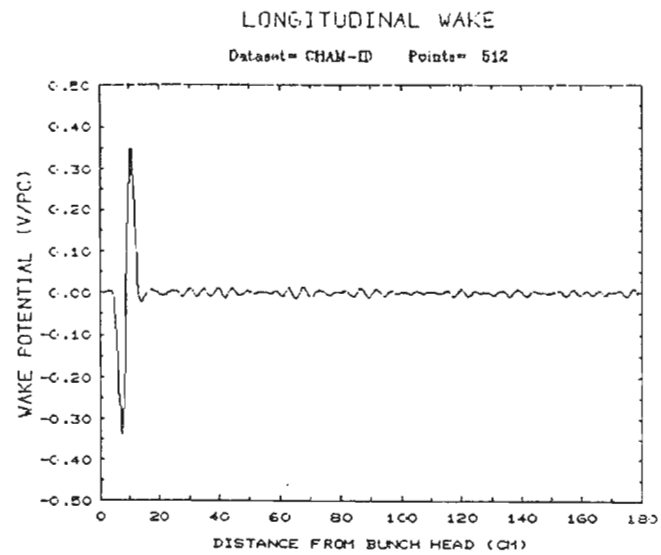
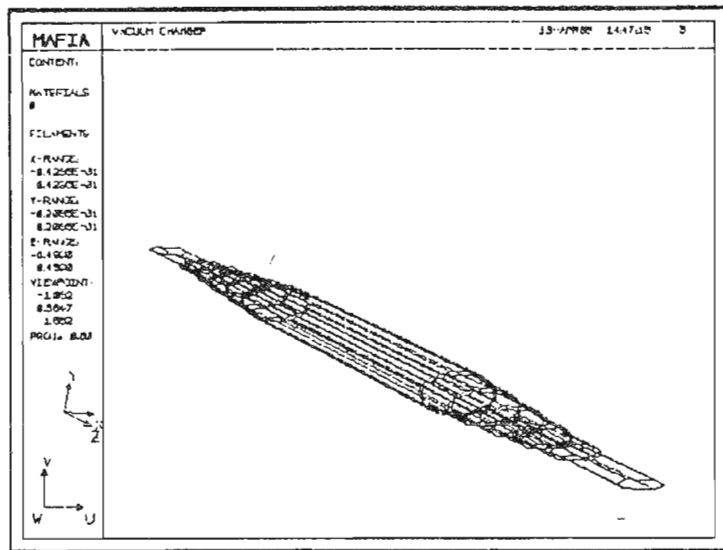


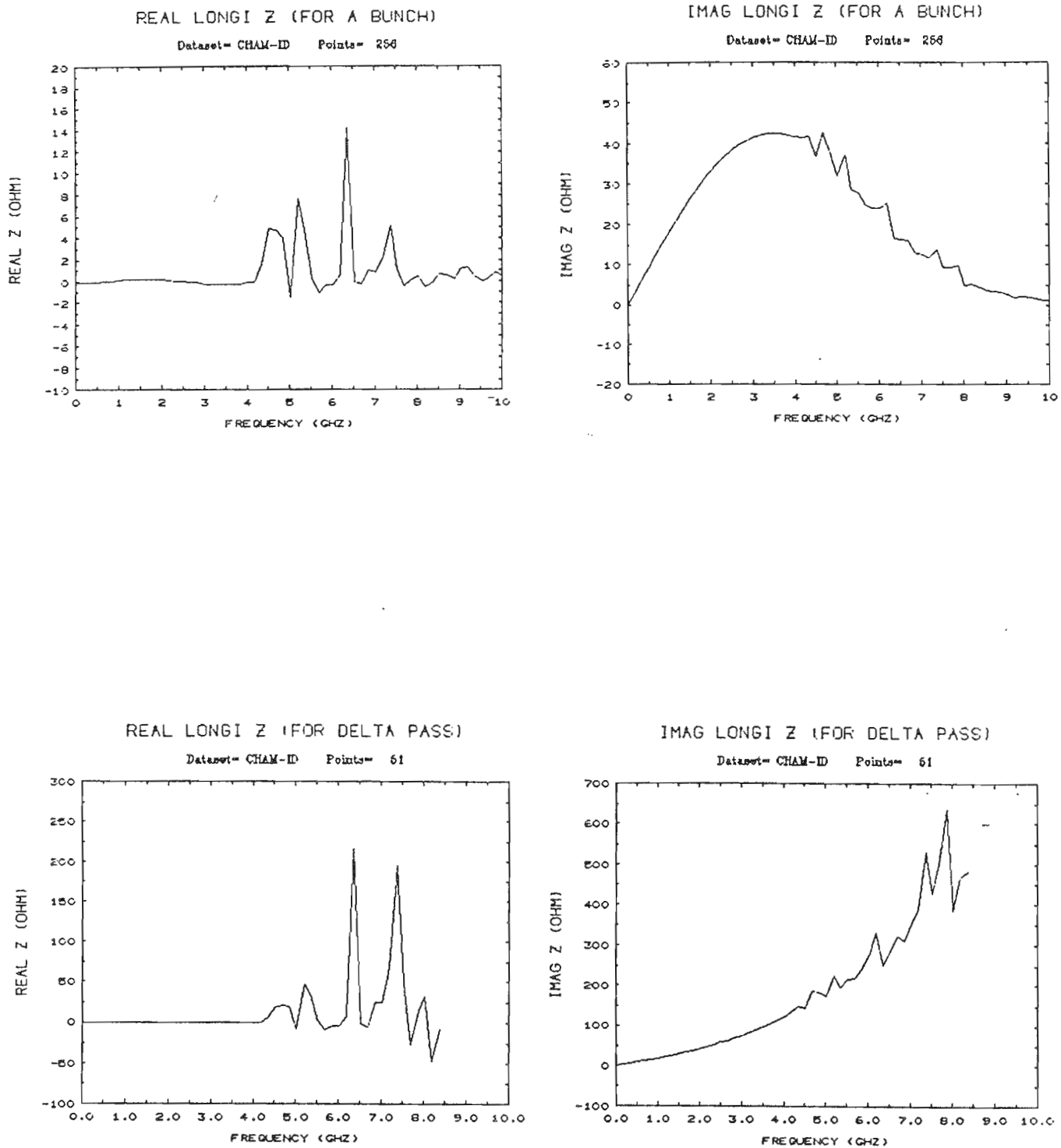
IMAG TRANS-V Z (FOR DELTA PASS)

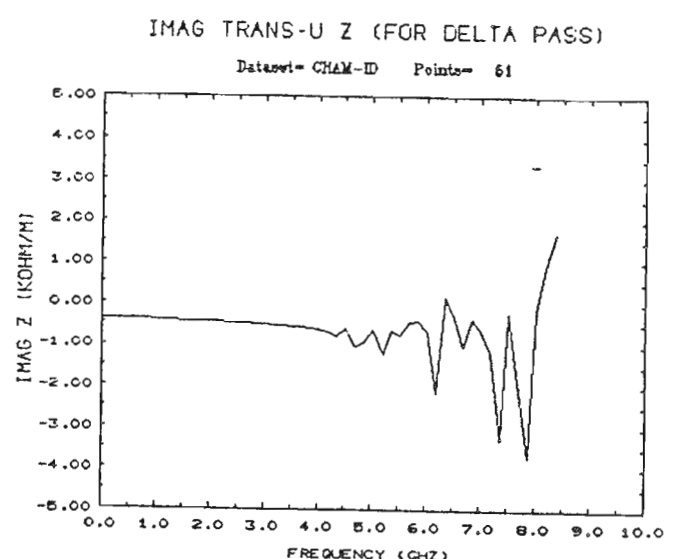
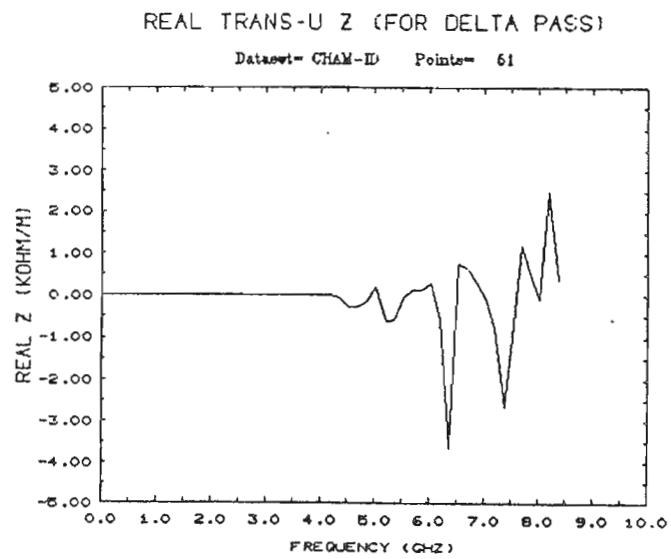
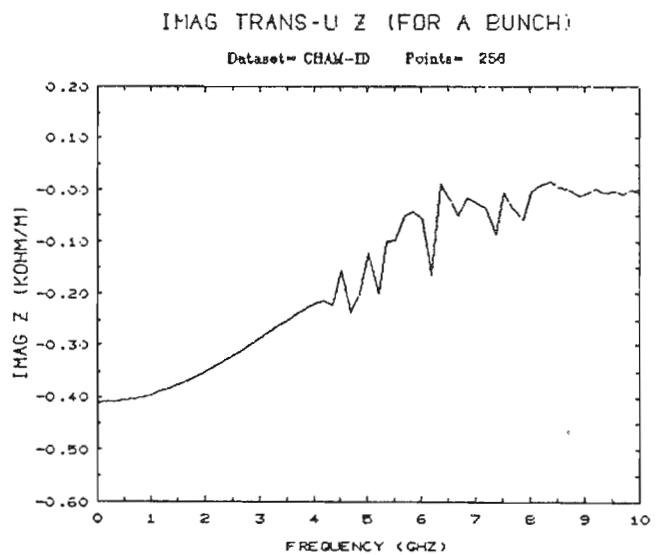
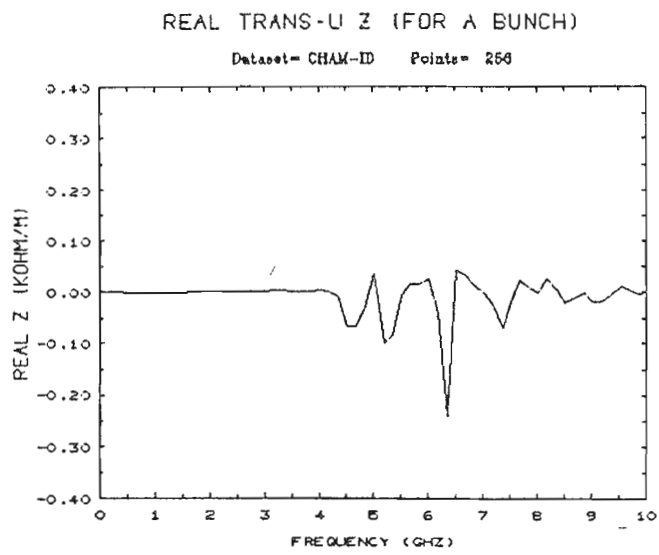
Dataset= ANTECHAM Points= 61

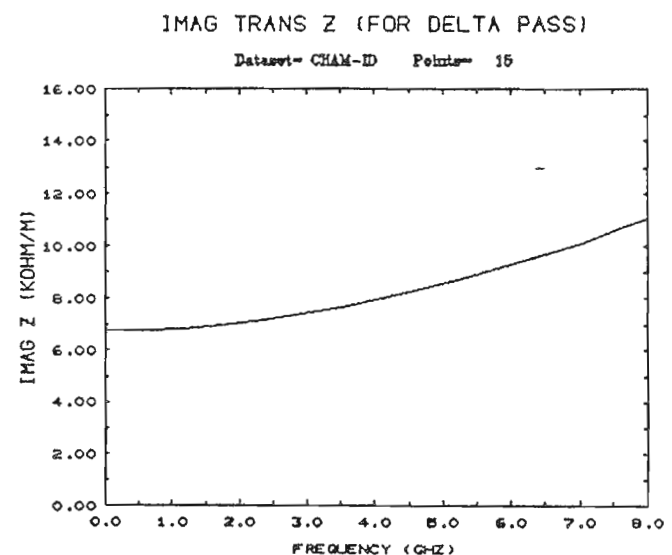
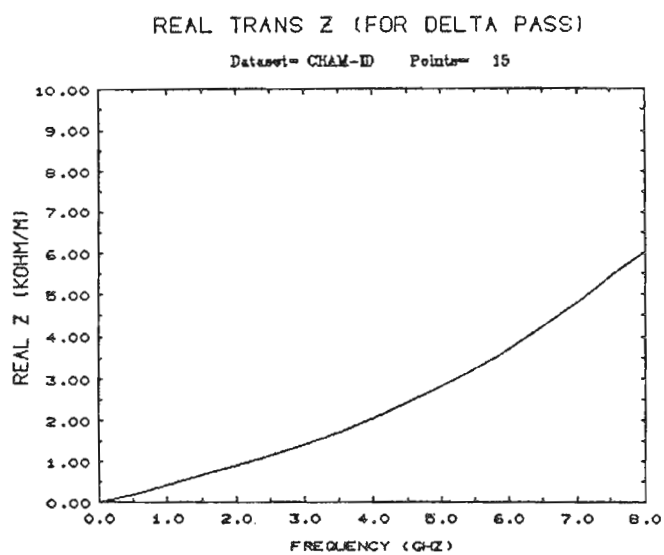
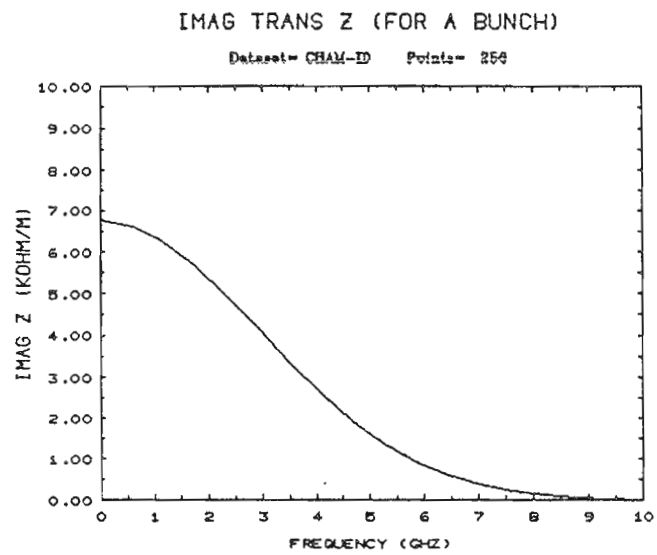
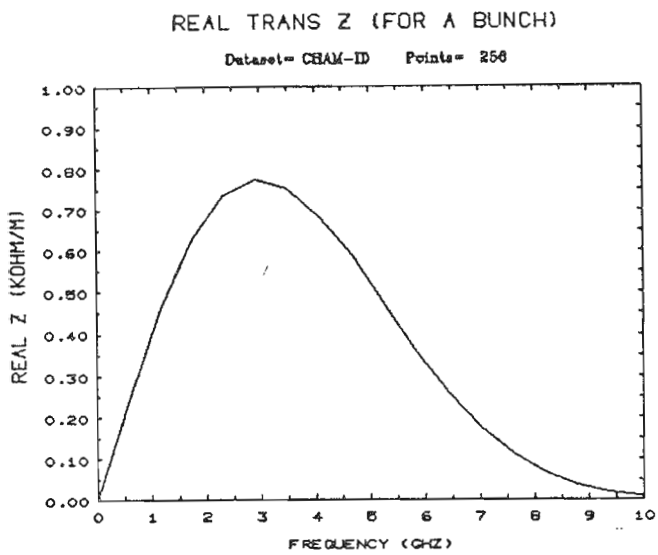


2. TRANSITION BETWEEN BEAM CHAMBER AND INSERTION DEVICE (ID) SECTION.

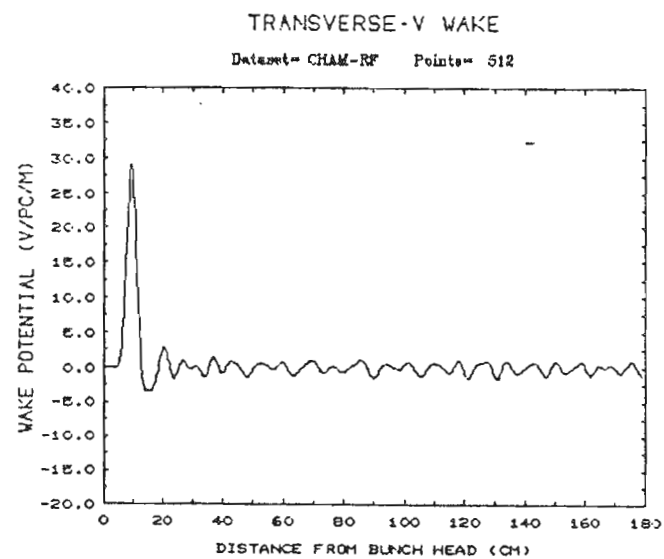
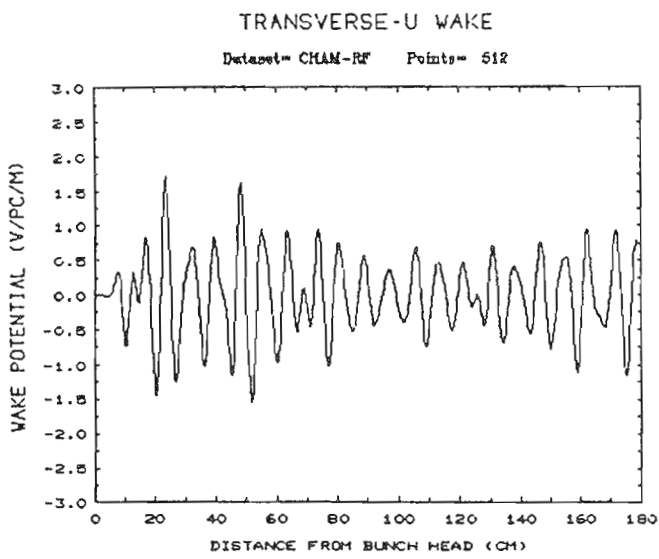
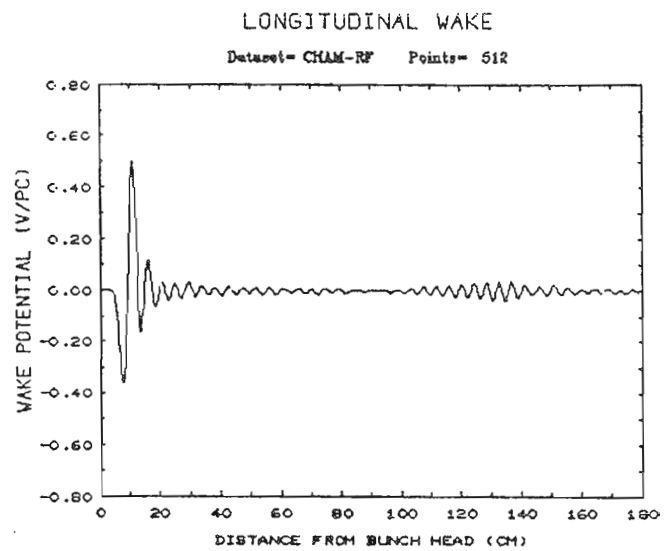
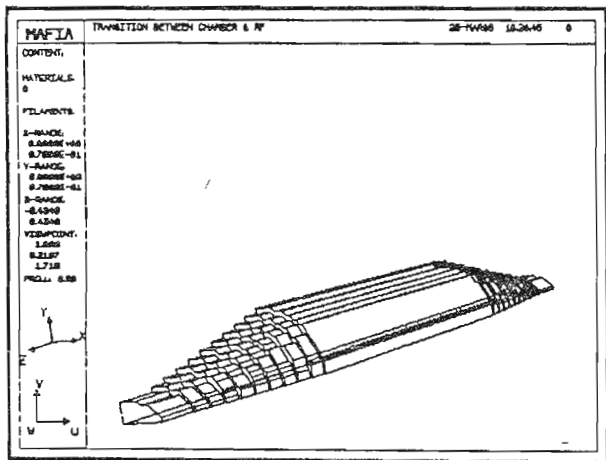


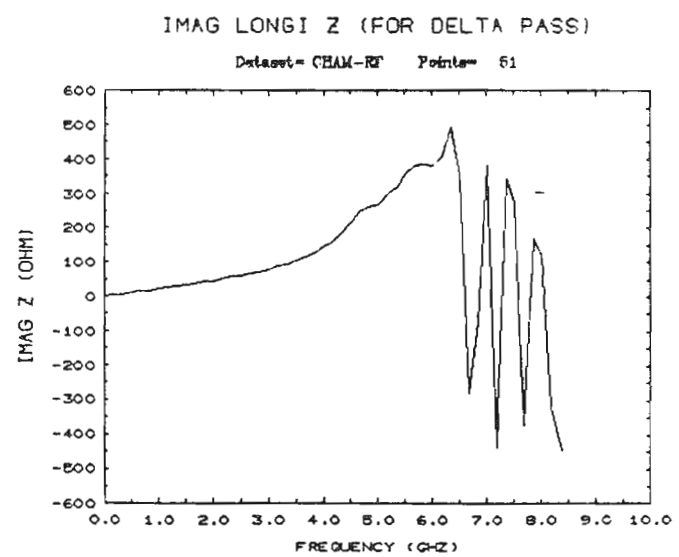
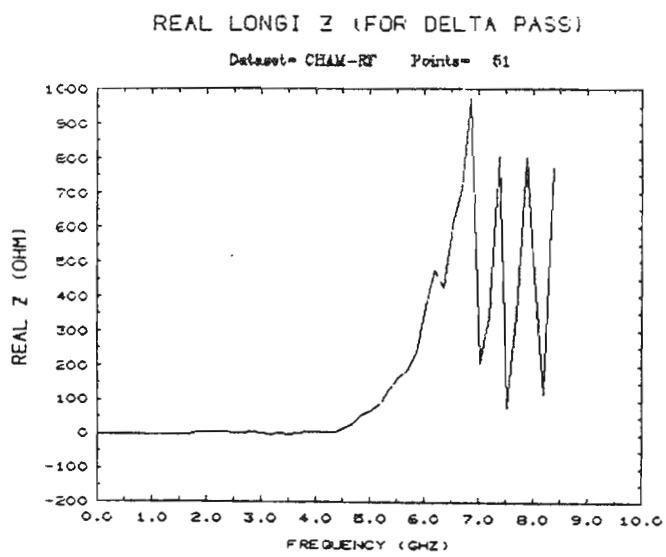
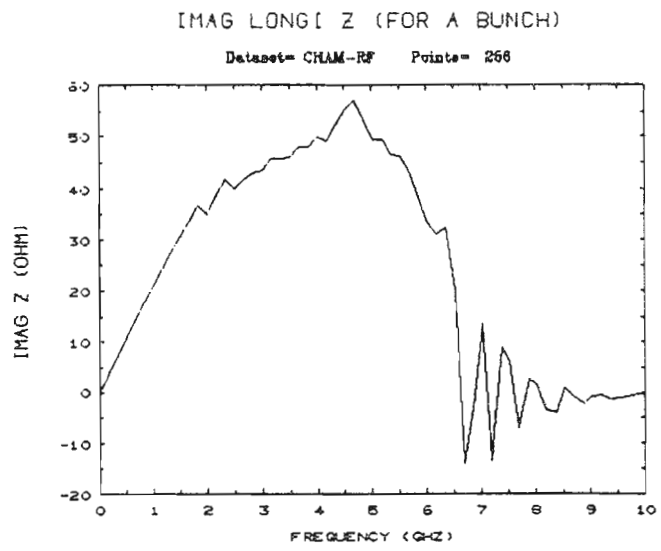
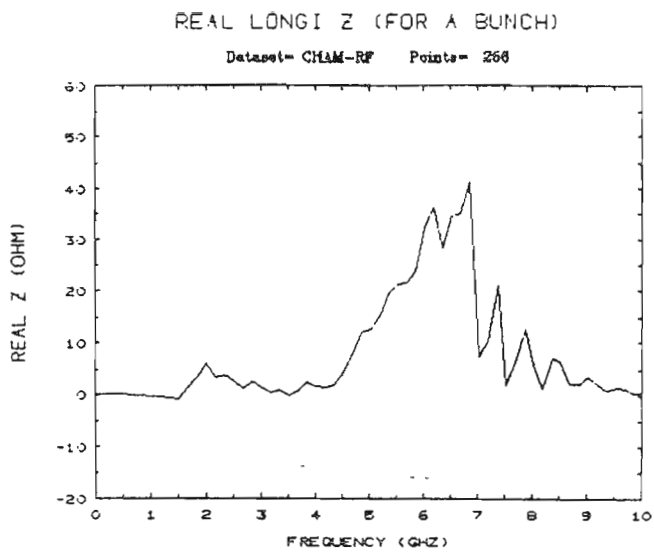


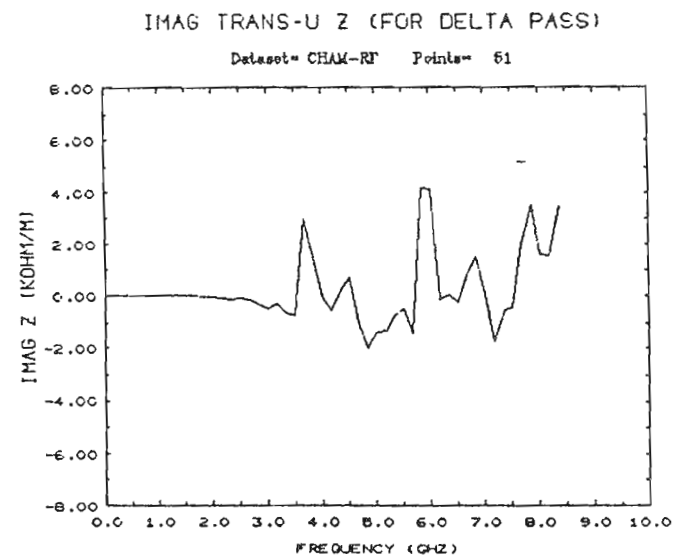
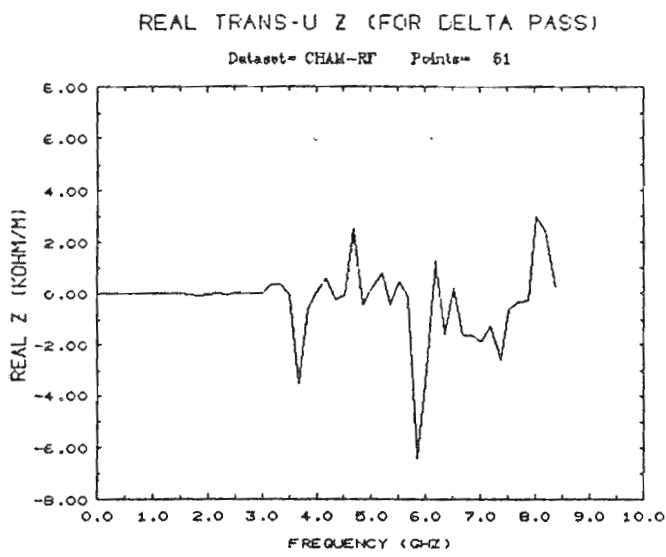
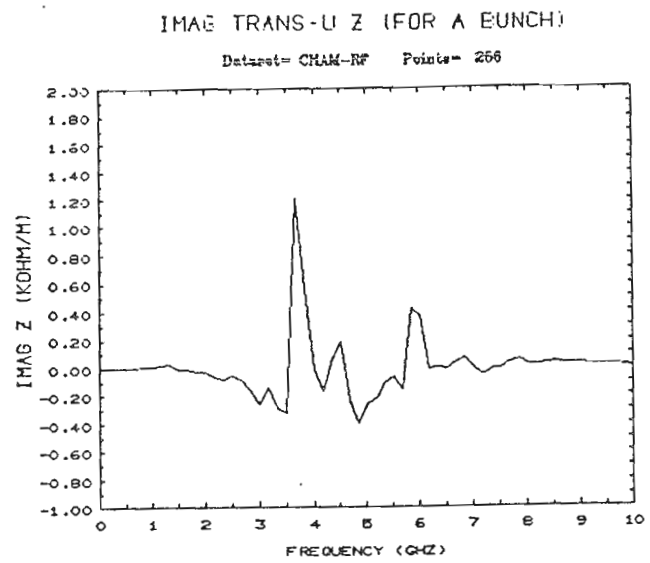
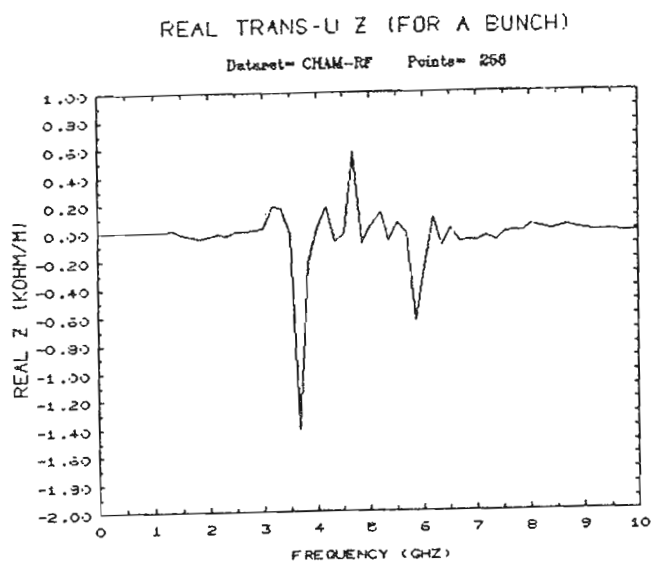


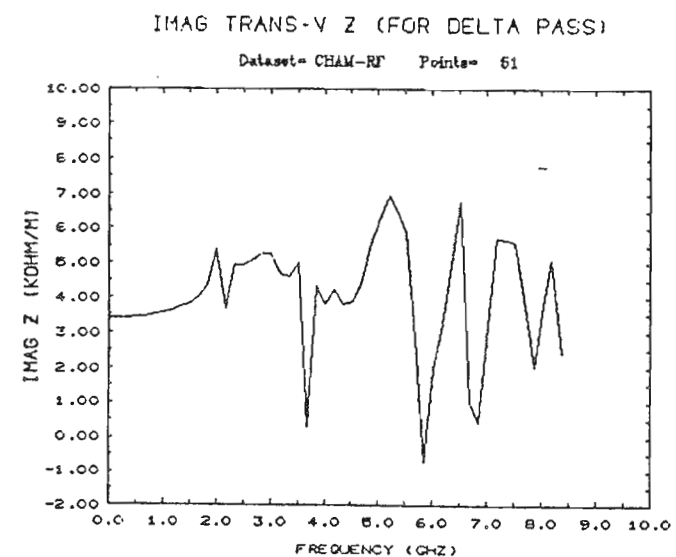
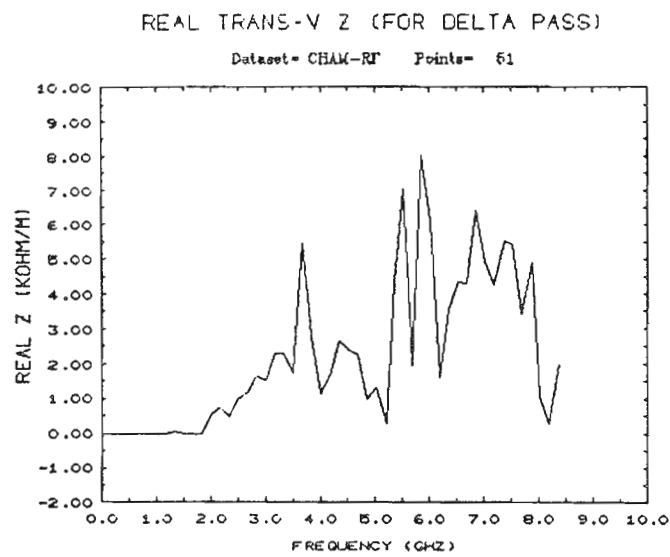
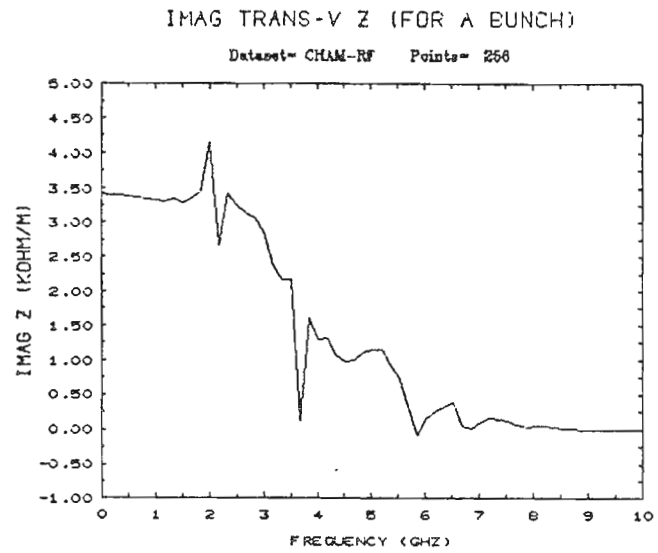
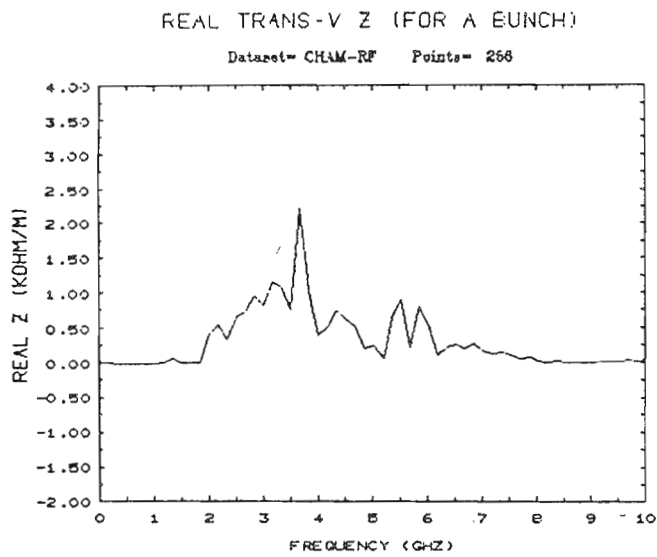


3. TRANSITION BETWEEN BEAM CHAMBER AND RF SECTION.

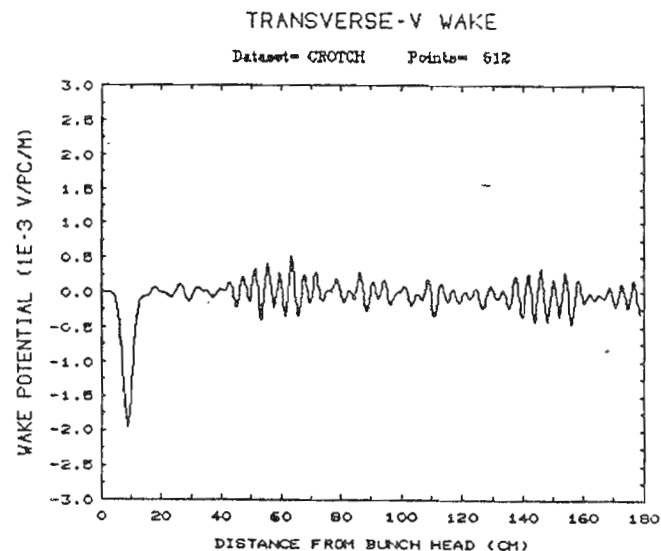
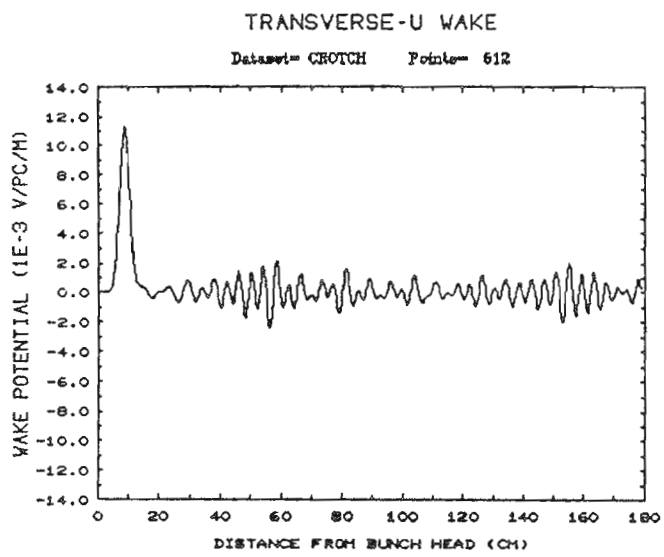
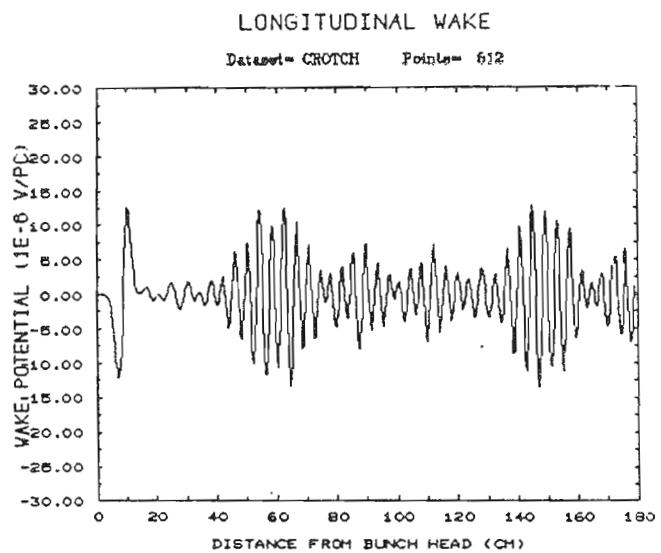
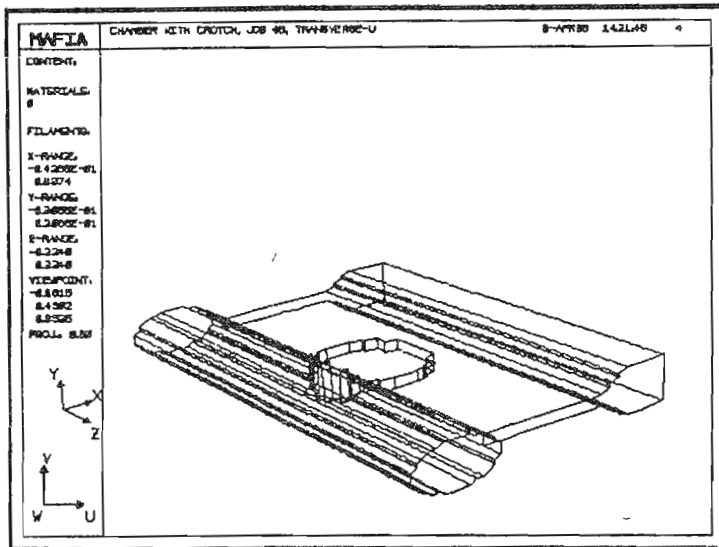


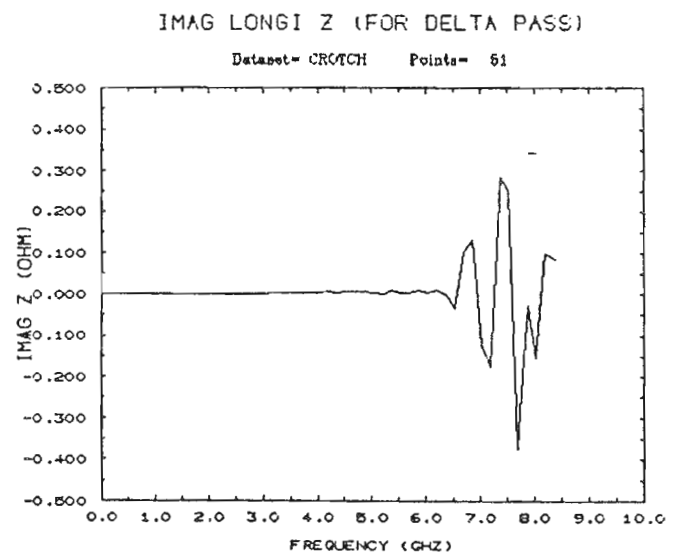
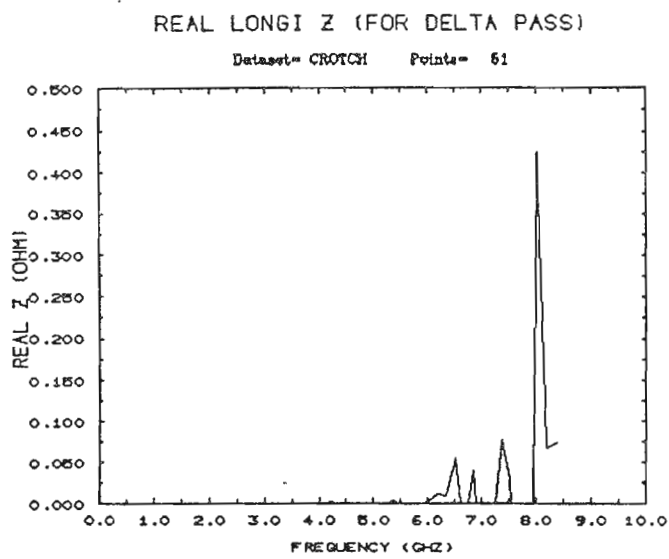
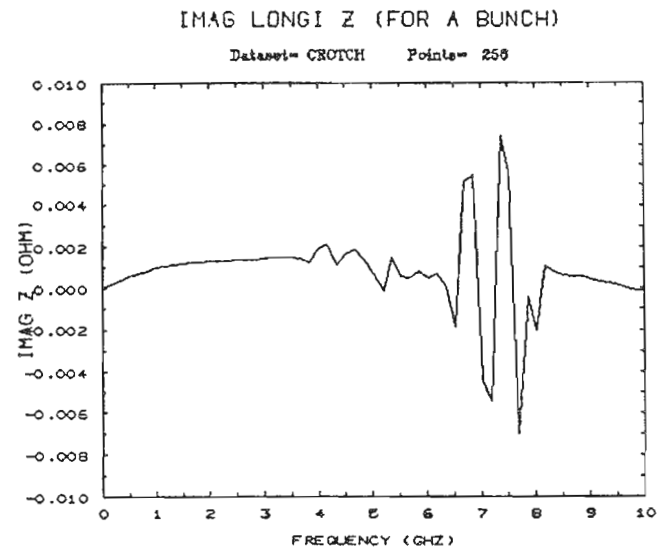
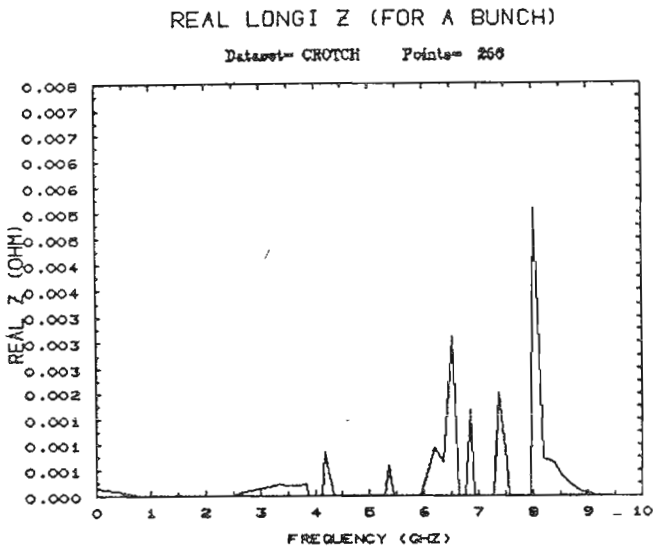


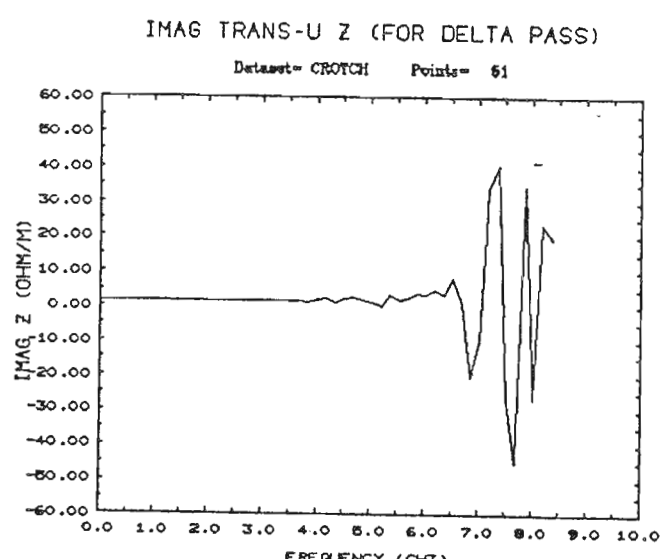
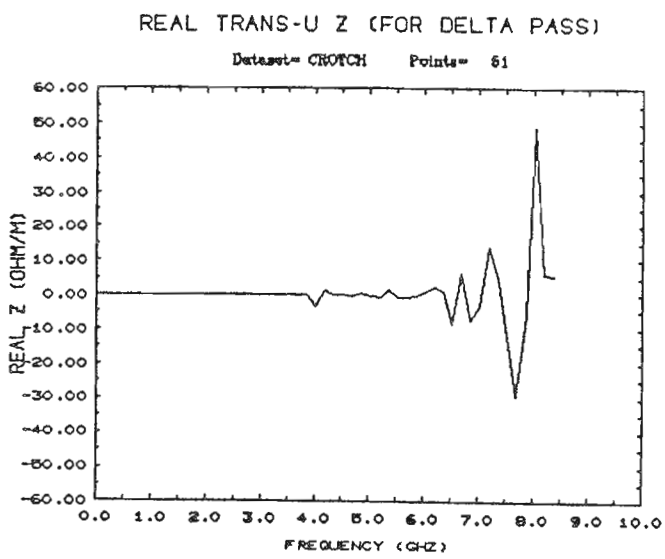
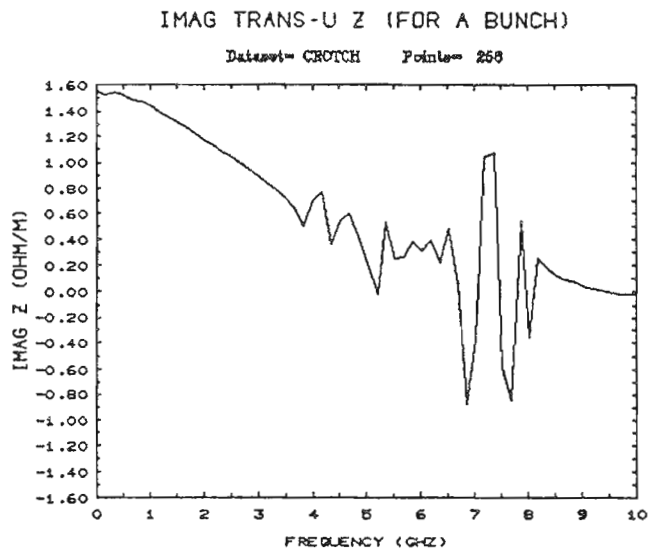
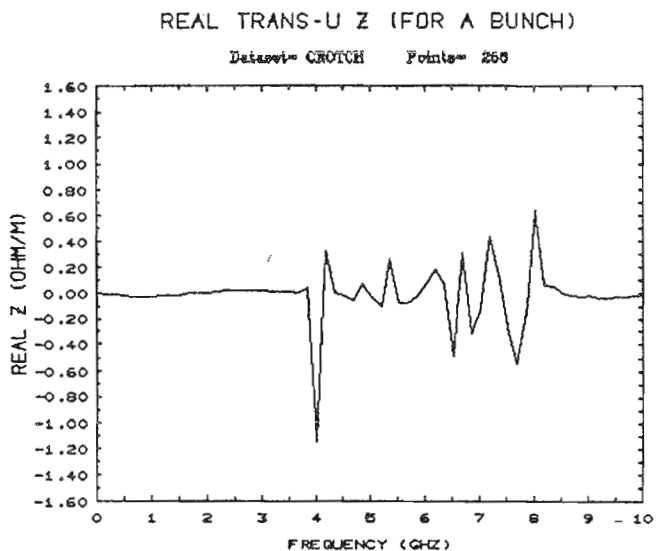




4. CROTCH ABSORBER.

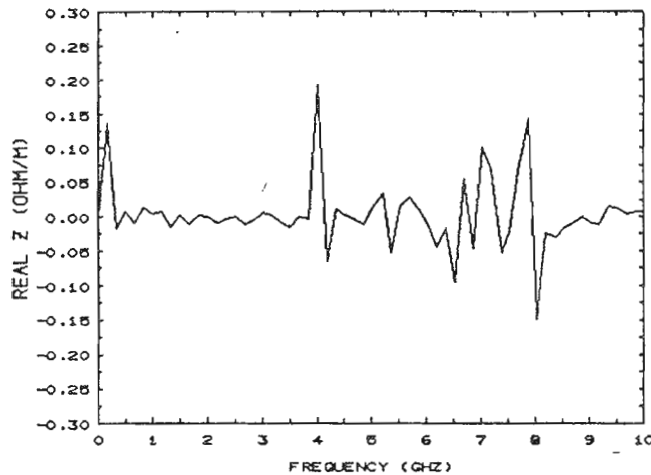






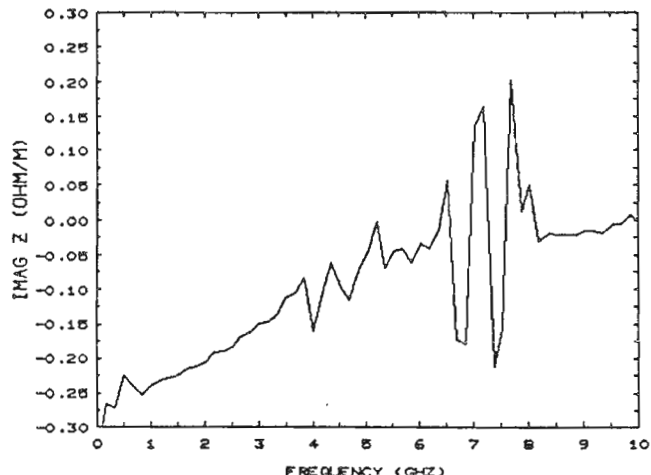
REAL TRANS-V Z (FOR A BUNCH)

Dataset= CROTCH Points= 256



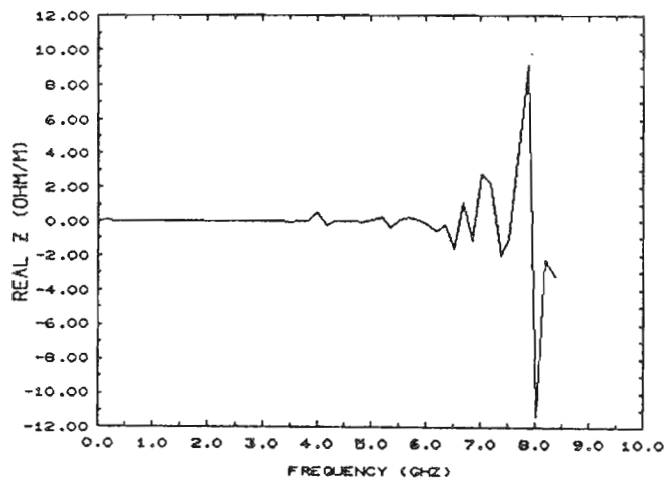
IMAG TRANS-V Z (FOR A BUNCH)

Dataset= CROTCH Points= 256



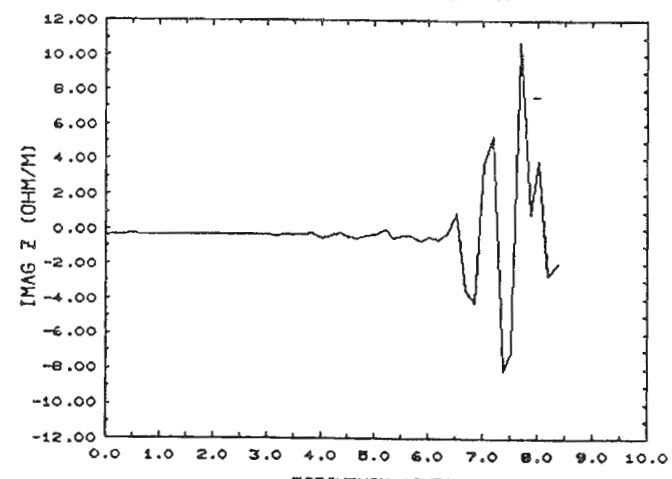
REAL TRANS-V Z (FOR DELTA PASS)

Dataset= CROTCH Points= 61

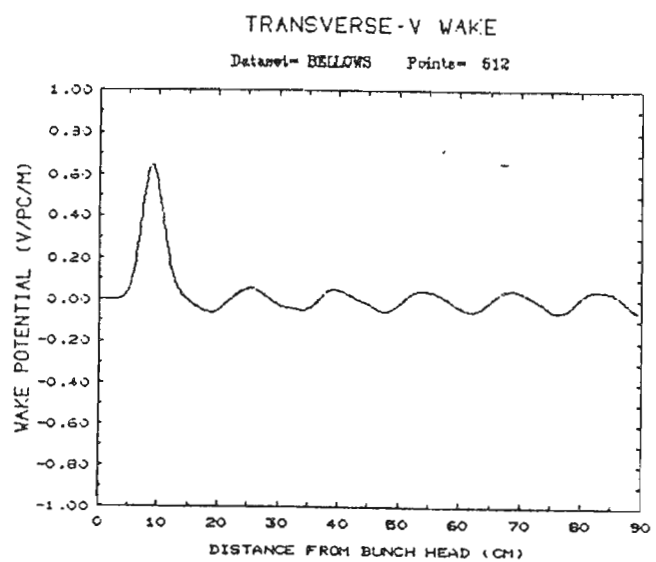
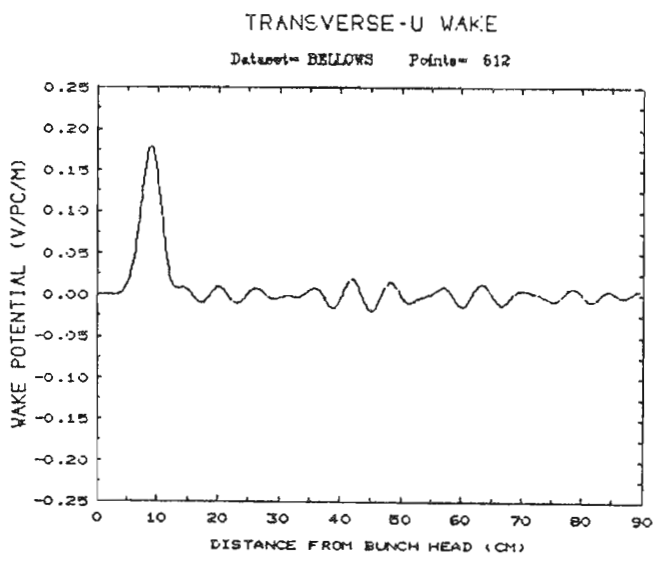
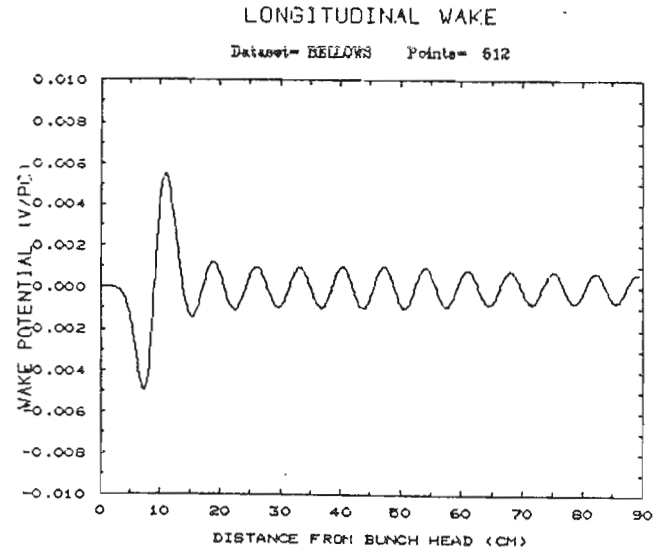
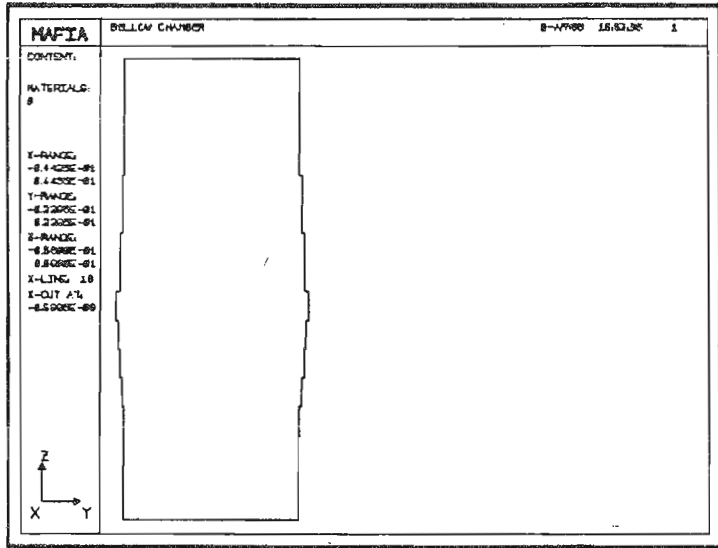


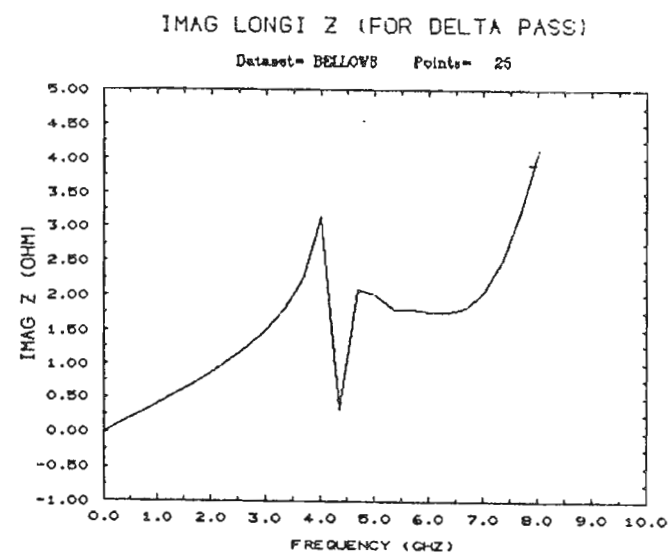
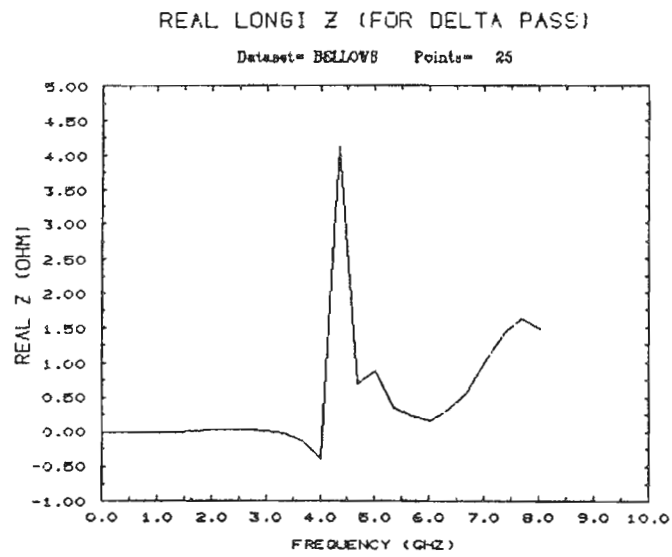
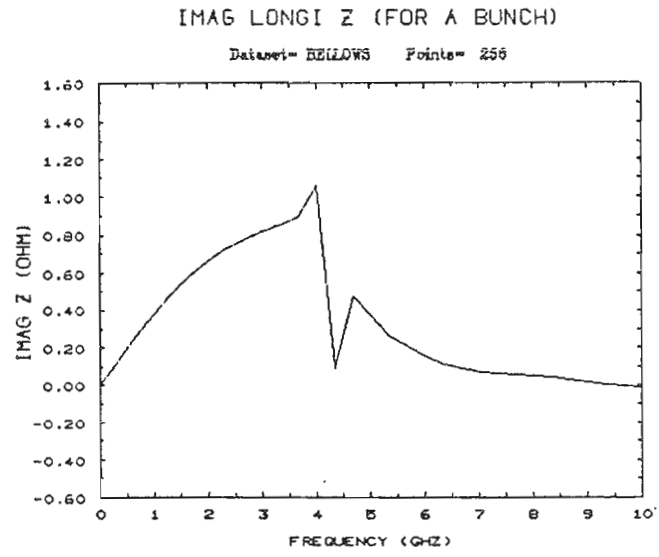
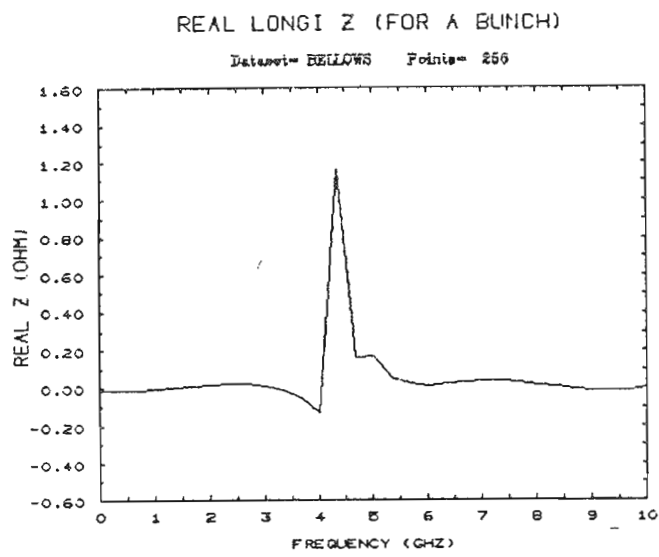
IMAG TRANS-V Z (FOR DELTA PASS)

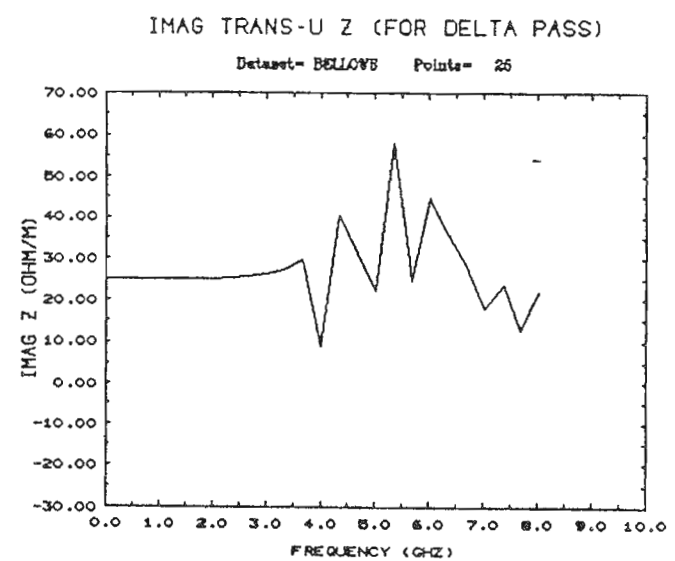
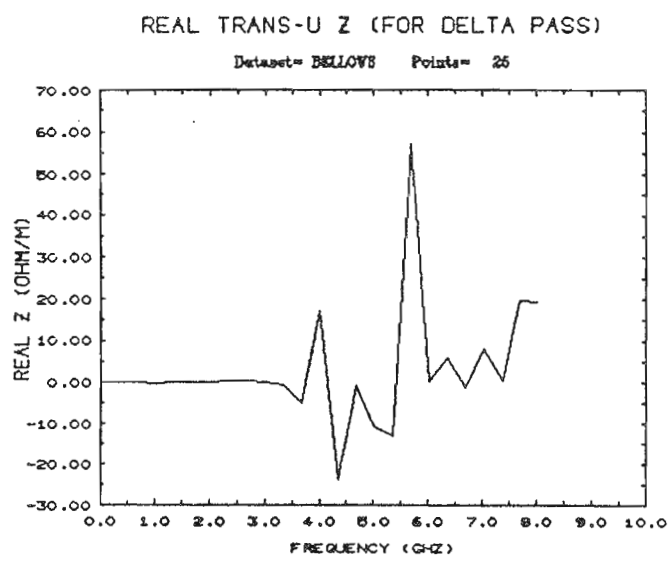
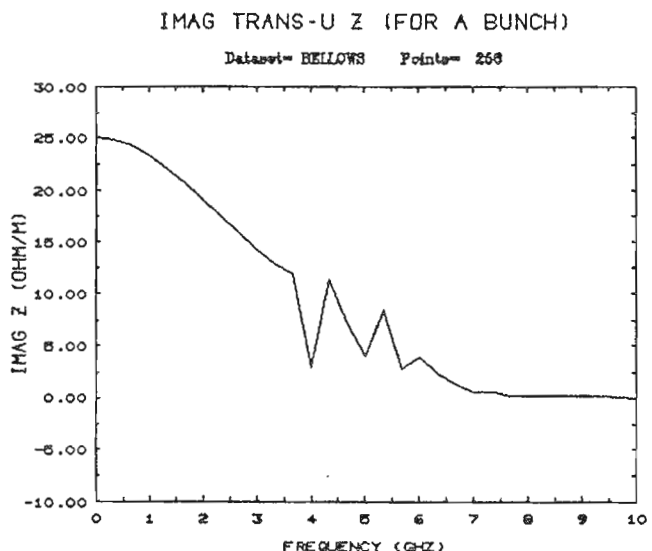
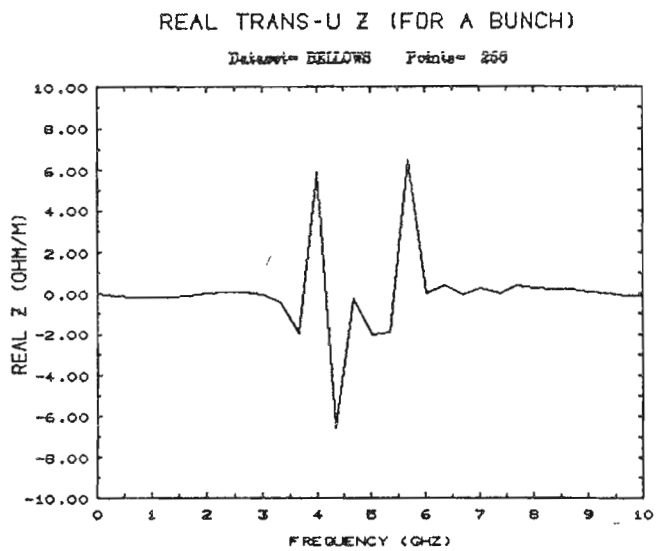
Dataset= CROTCH Points= 61

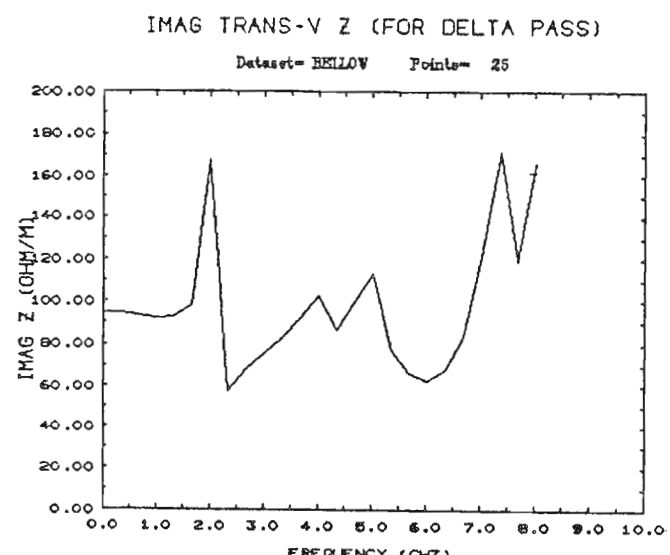
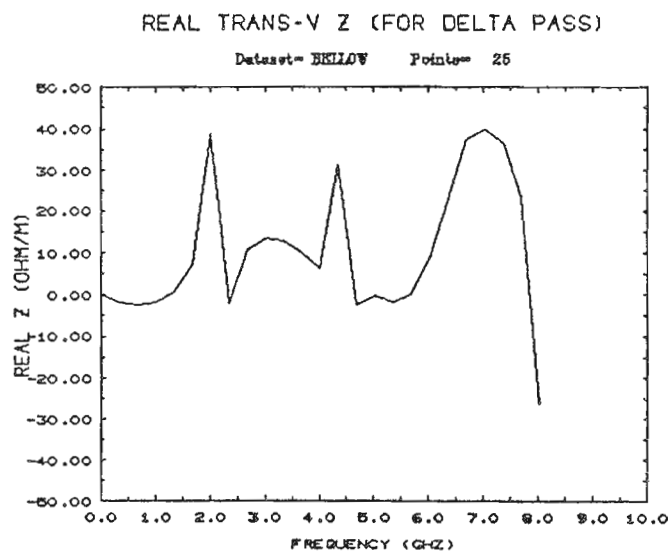
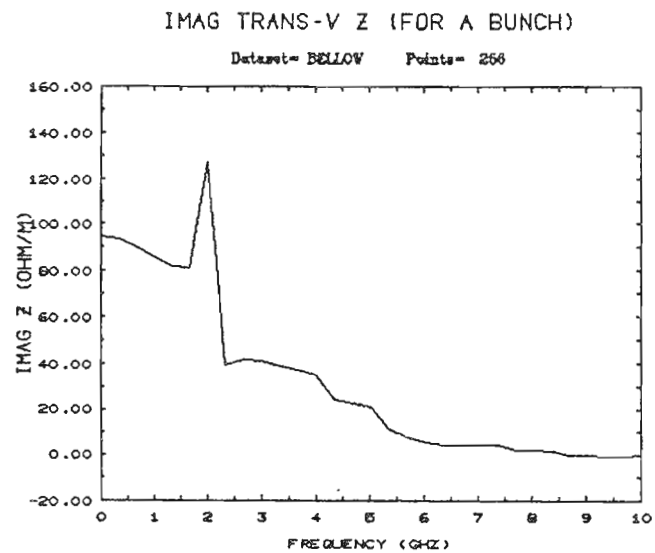
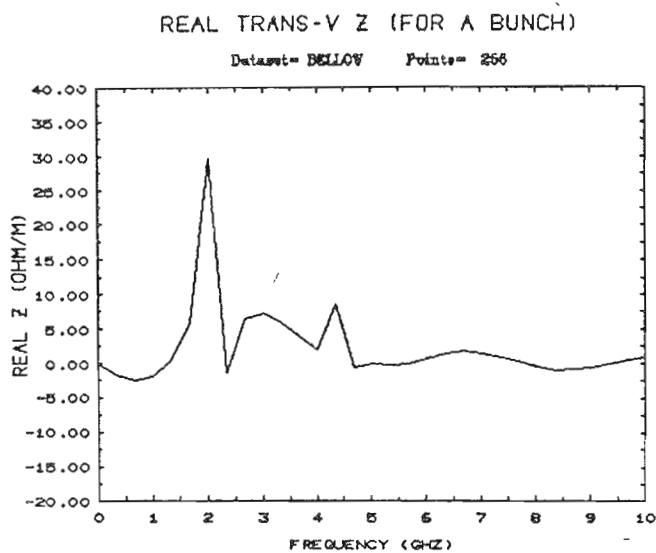


5. BELLOWS (SHIELDED).

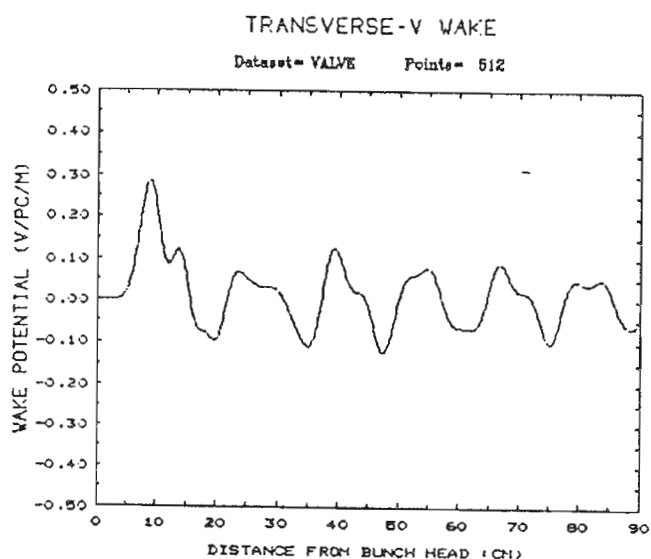
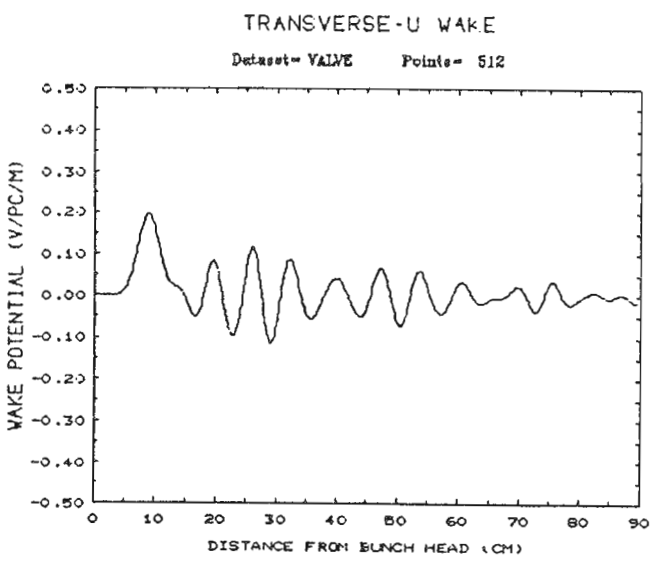
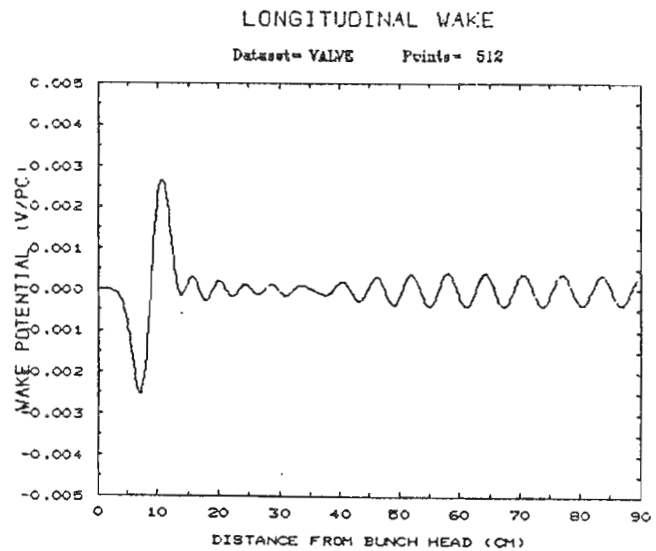
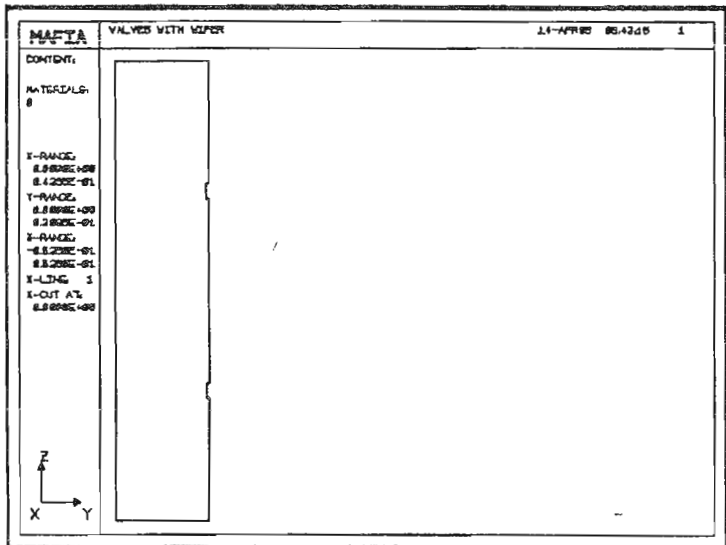






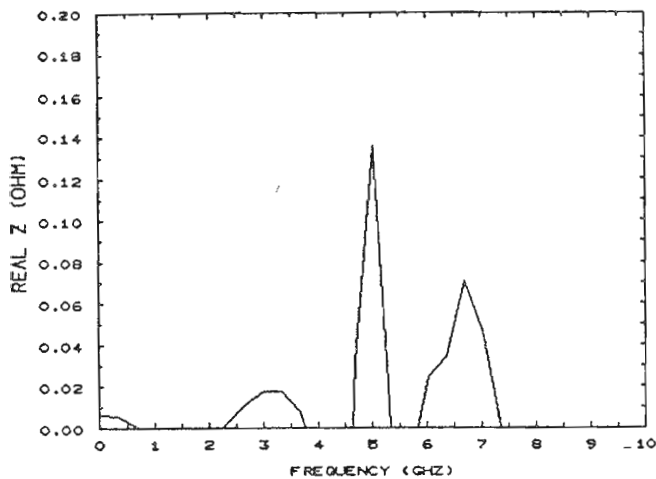


6. VALVE.



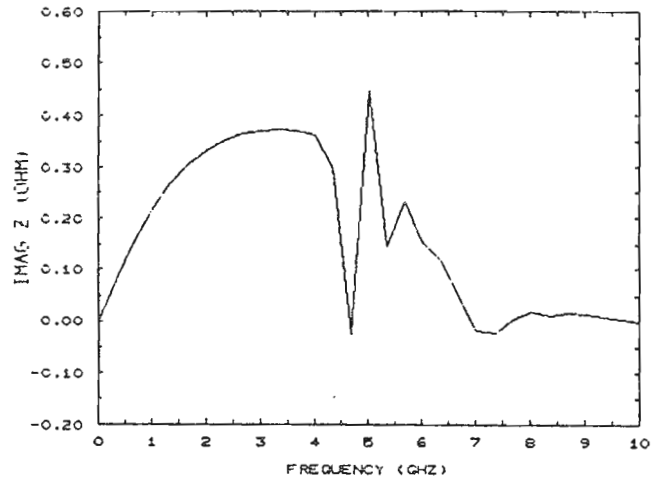
REAL LONGI Z (FOR A BUNCH)

Dataset= VALVE Points= 256



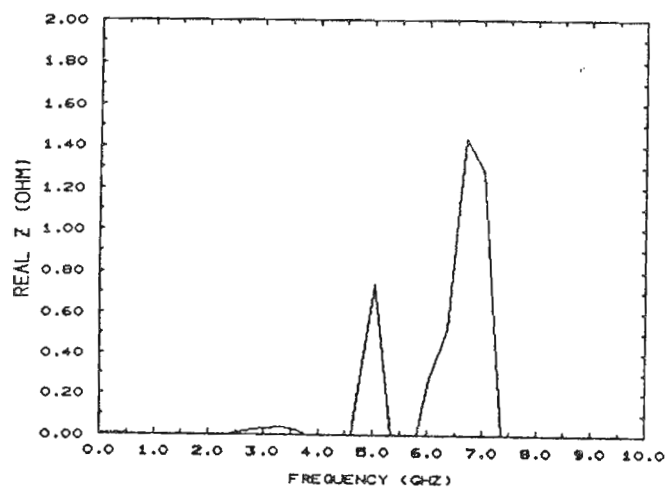
IMAG LONGI Z (FOR A BUNCH)

Dataset= VALVE Points= 256



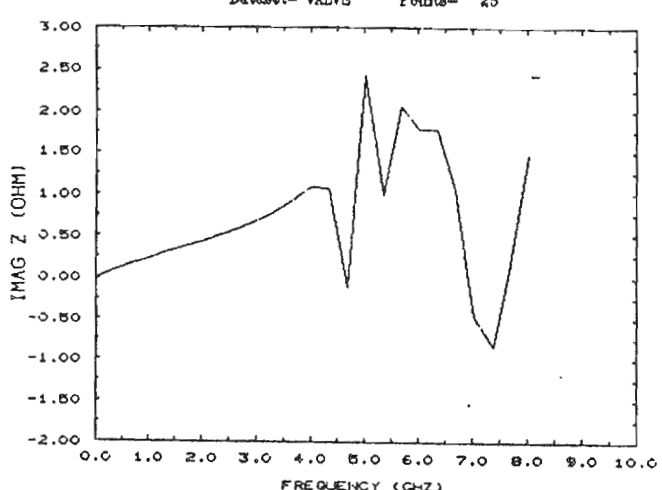
REAL LONGI Z (FOR DELTA PASS)

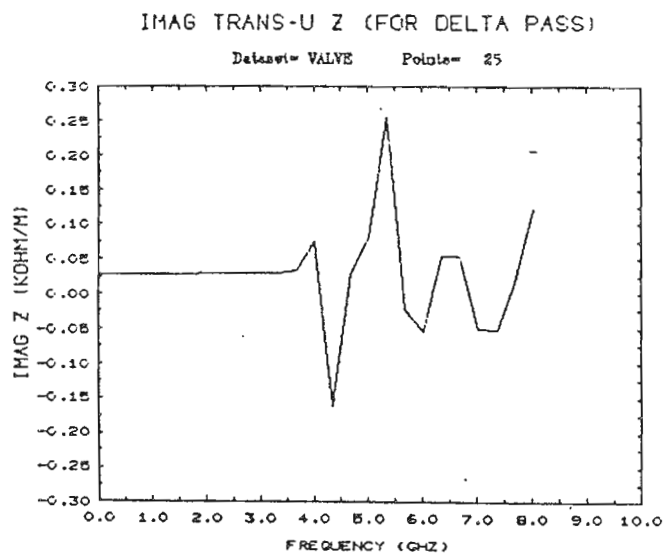
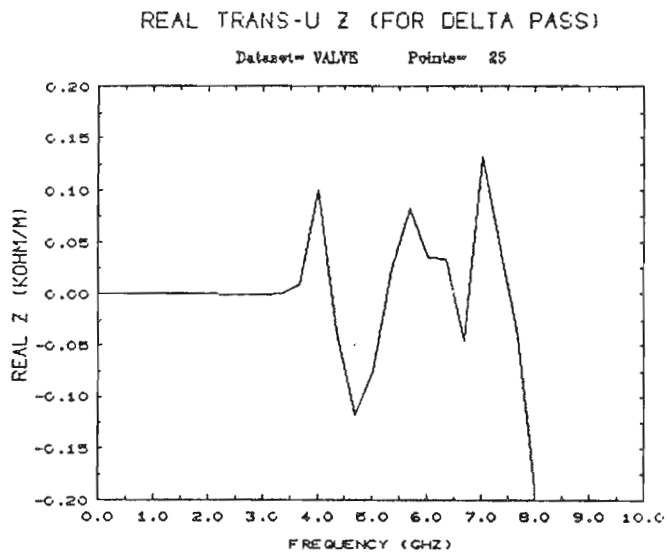
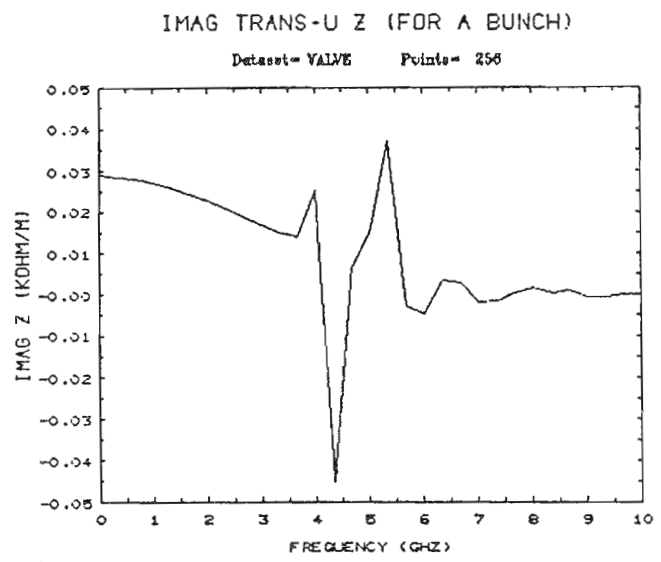
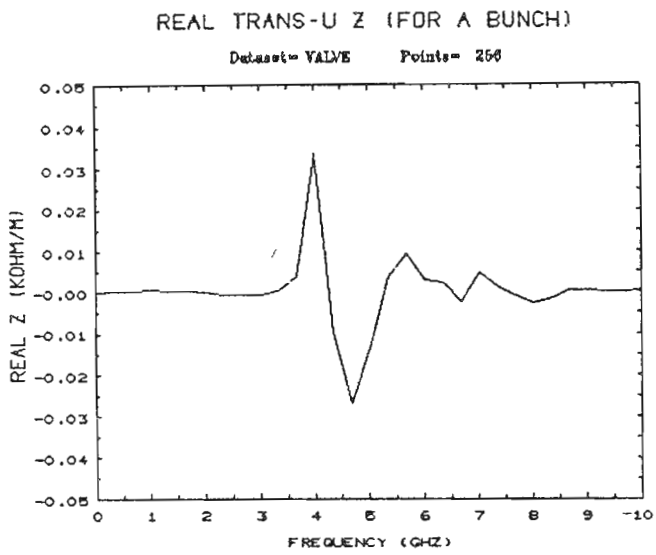
Dataset= VALVE Points= 25

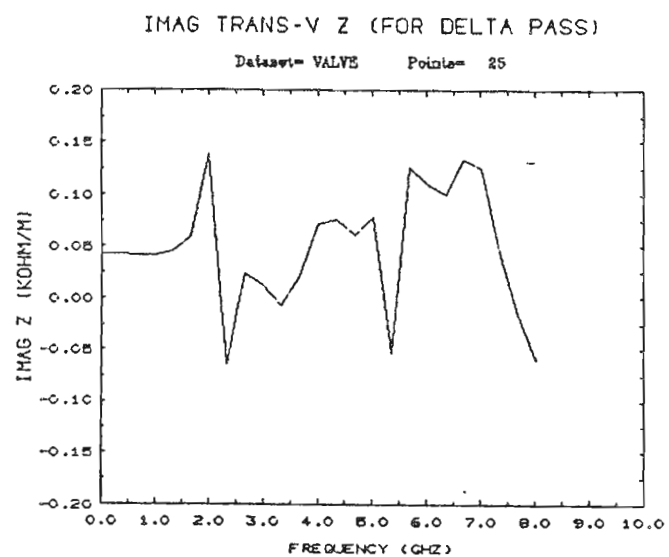
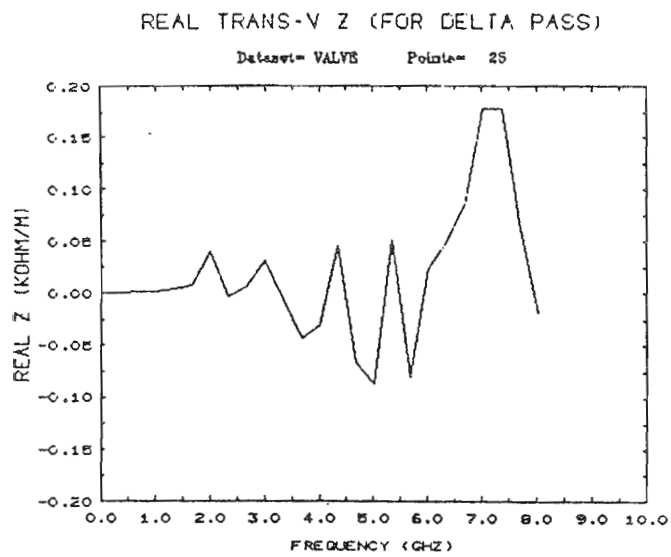
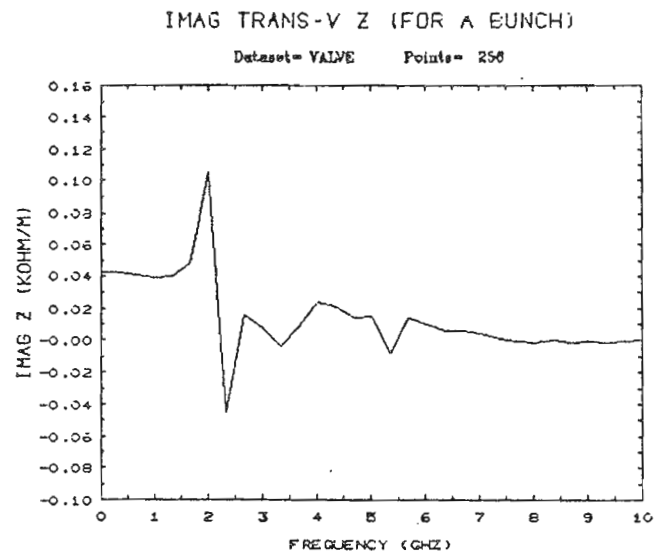
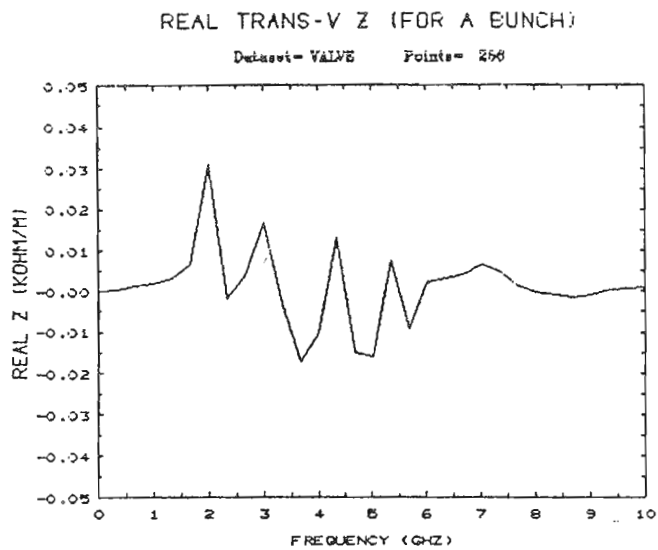


IMAG LONGI Z (FOR DELTA PASS)

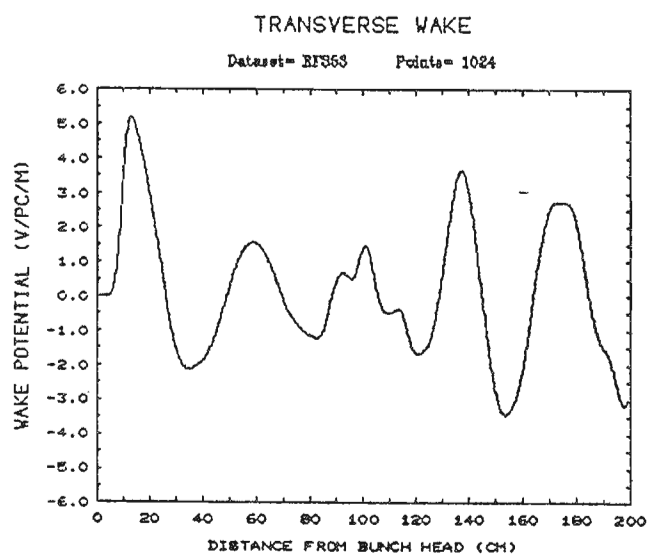
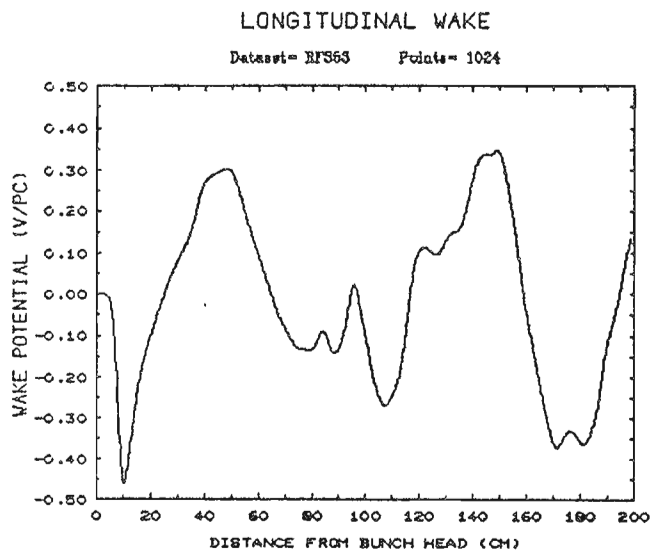
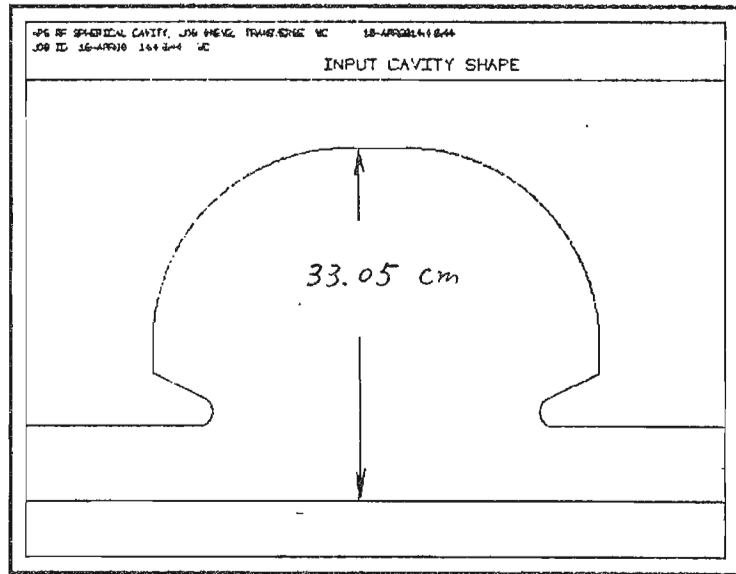
Dataset= VALVE Points= 25

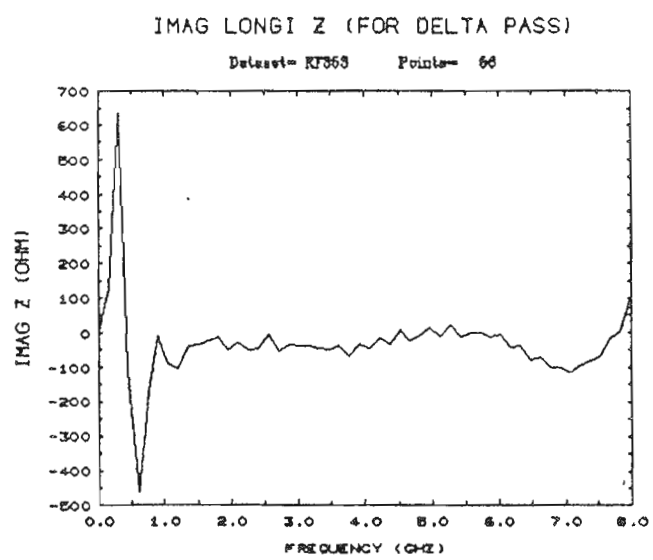
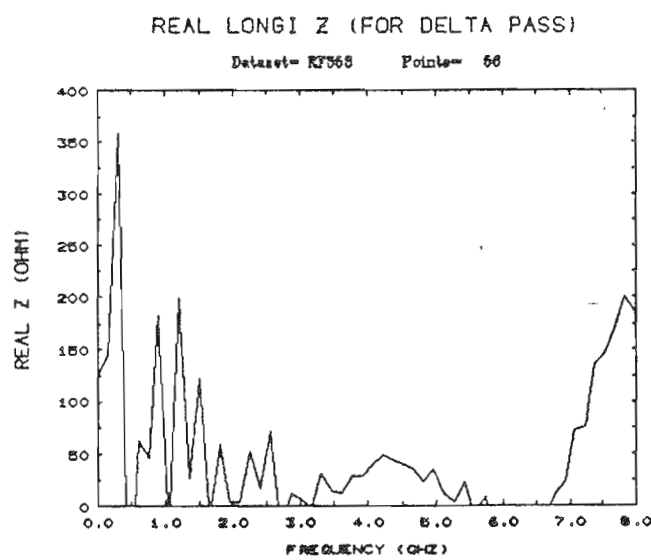
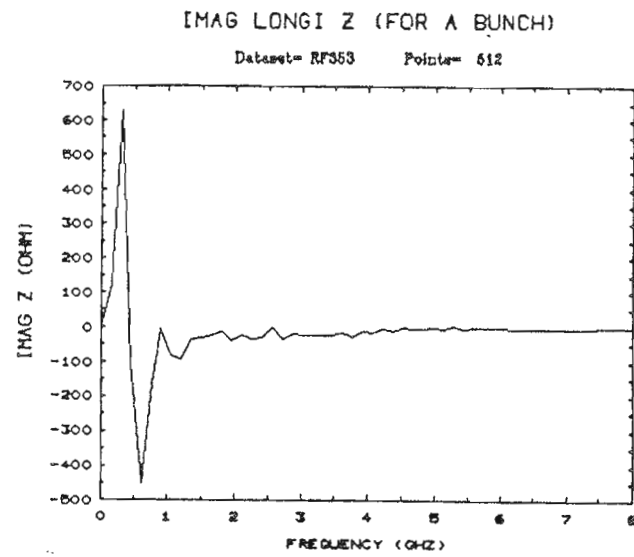
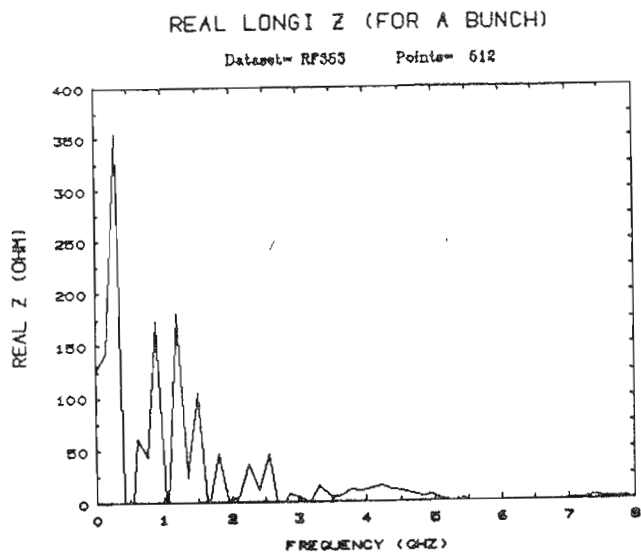


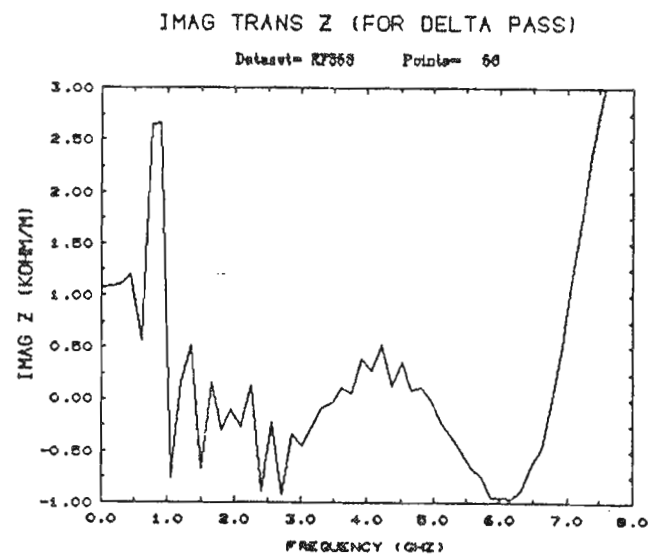
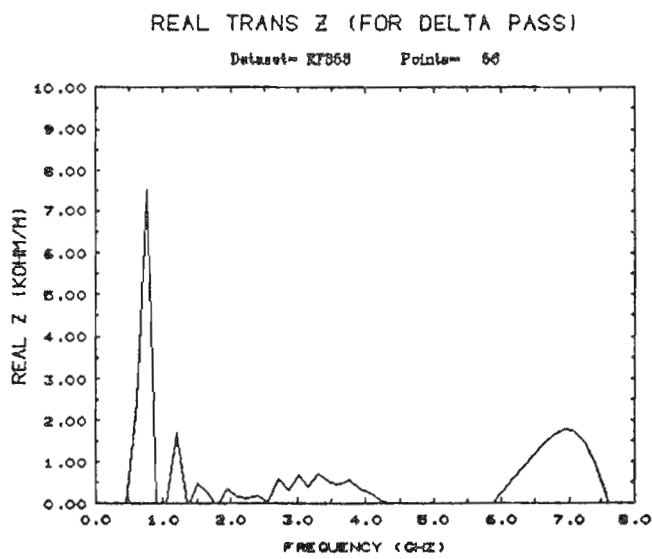
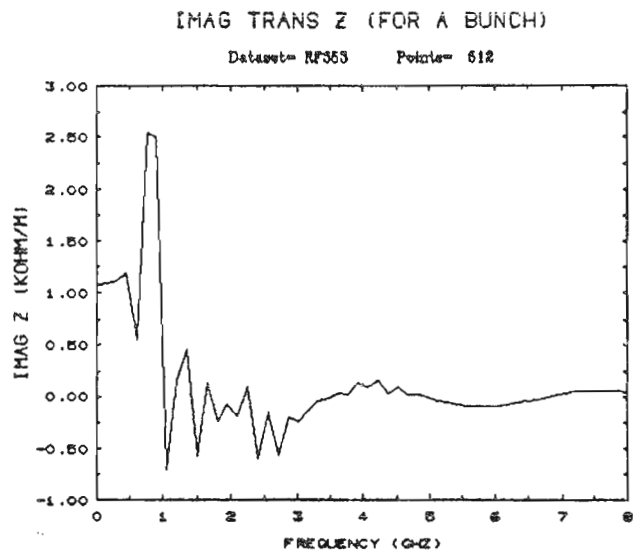
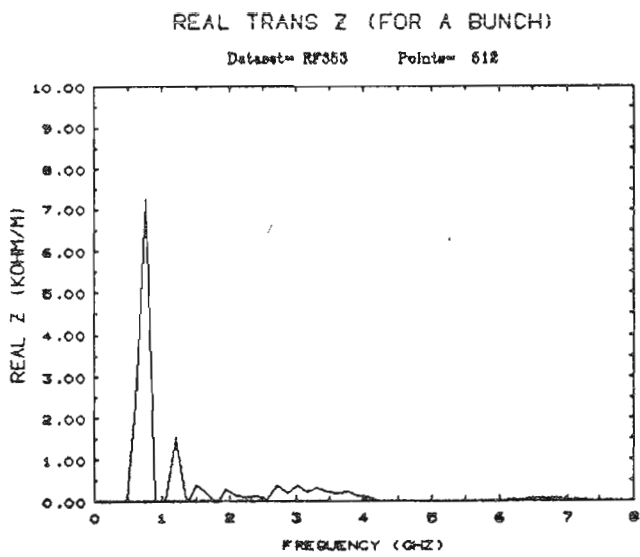




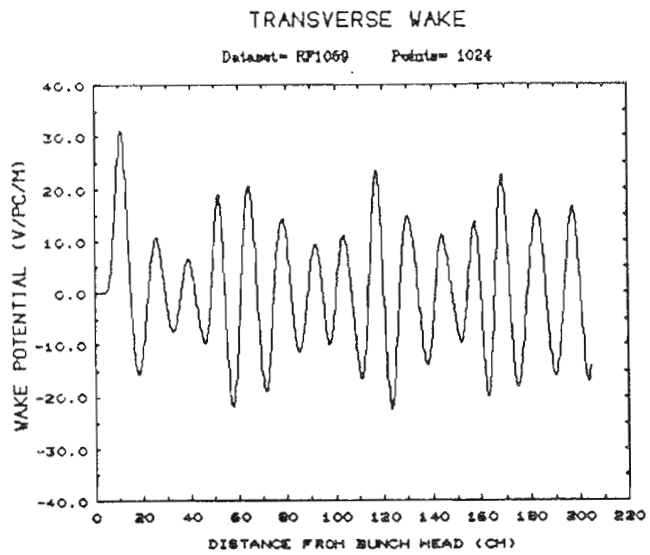
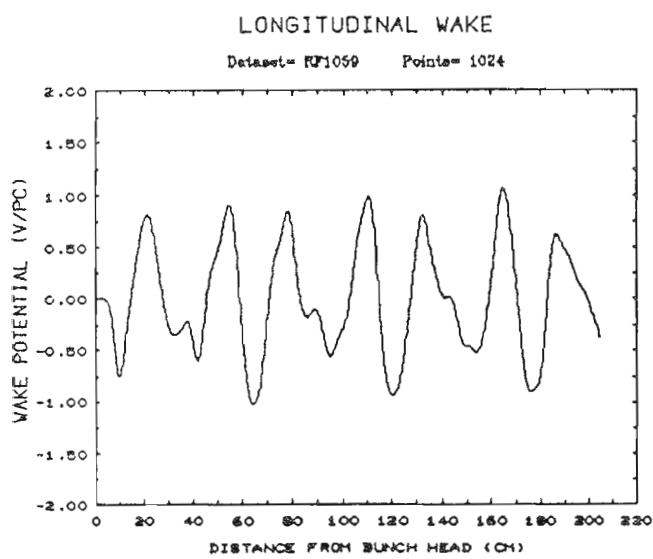
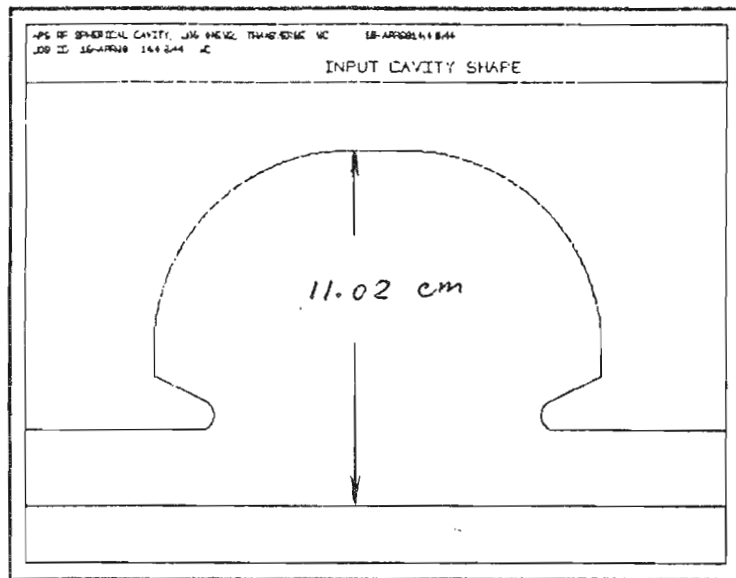
7. RF CAVITY (353 MHz).

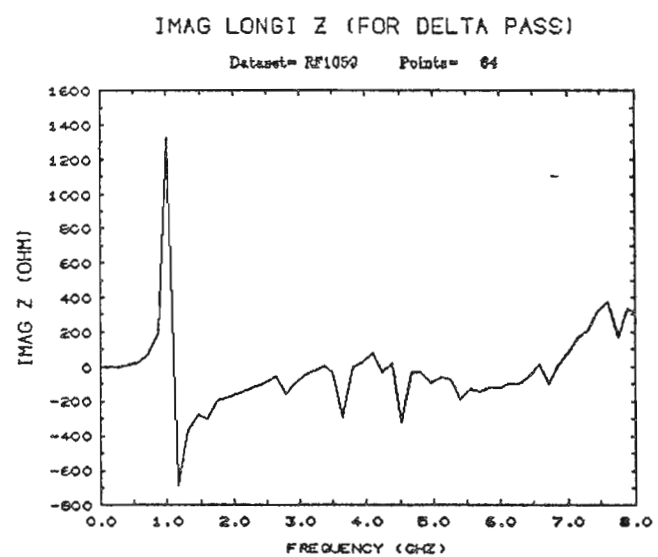
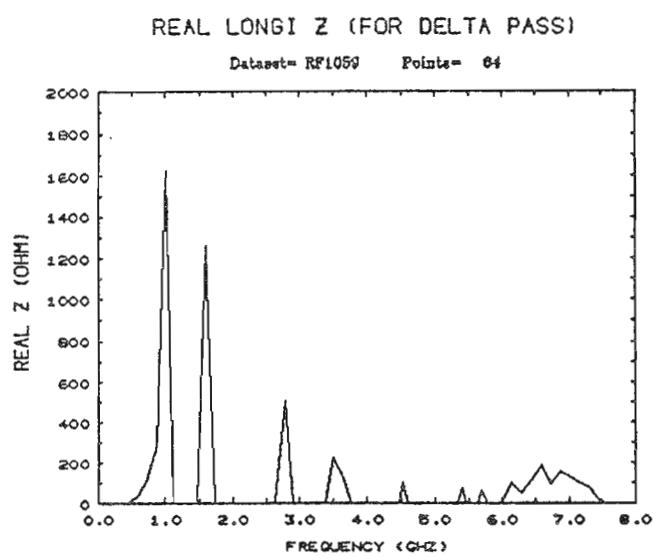
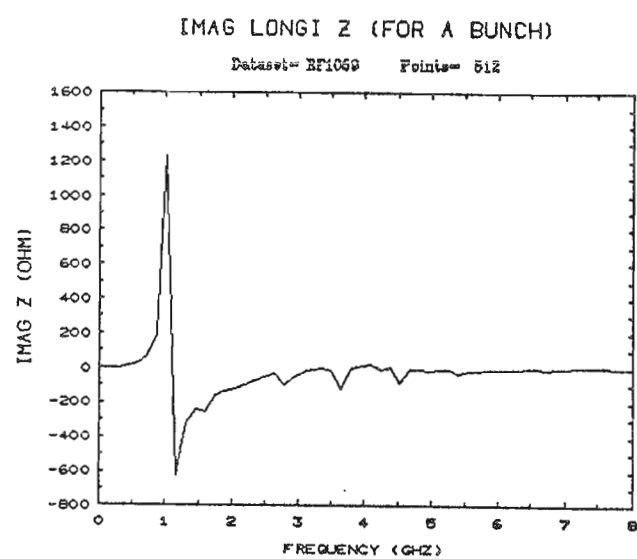
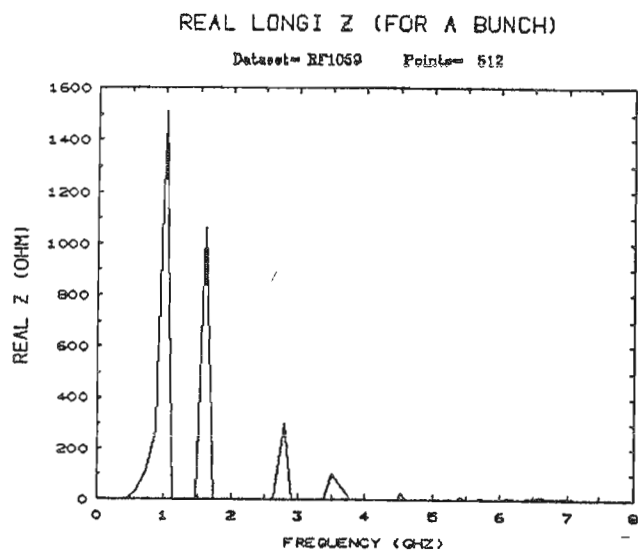


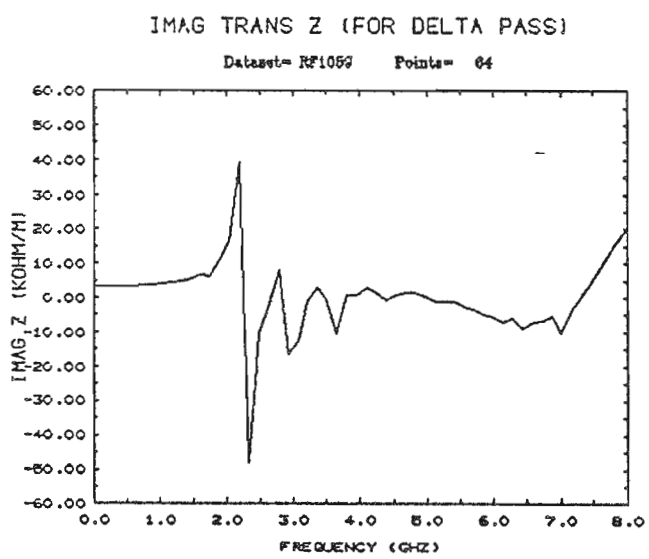
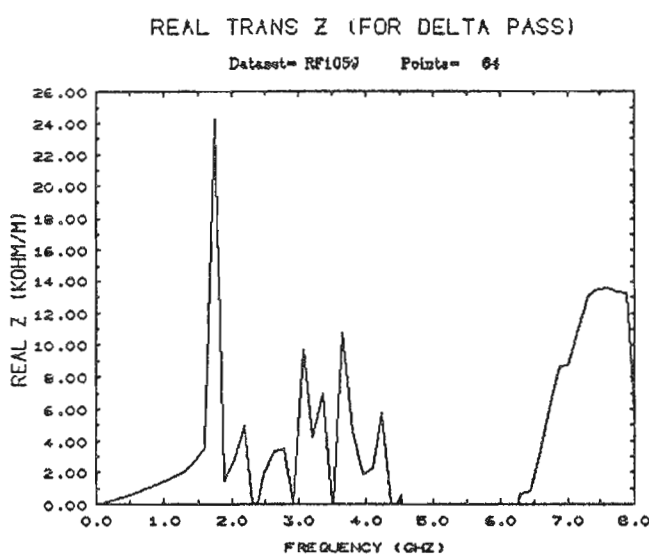
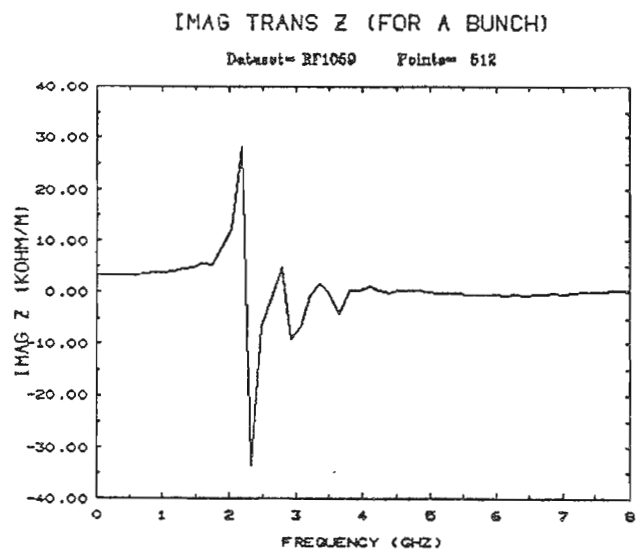
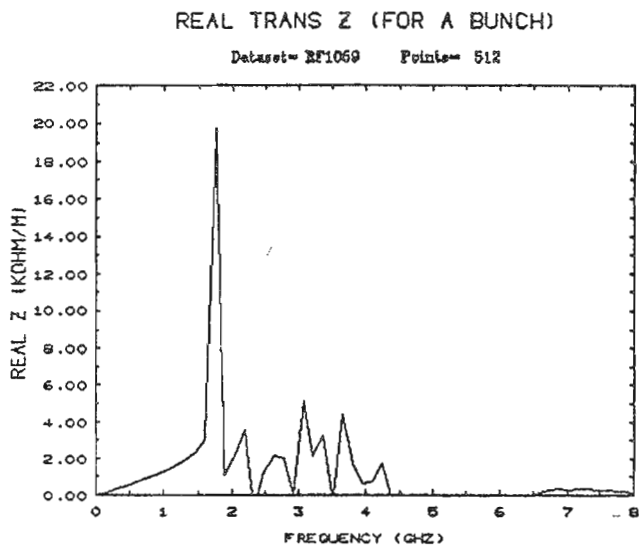




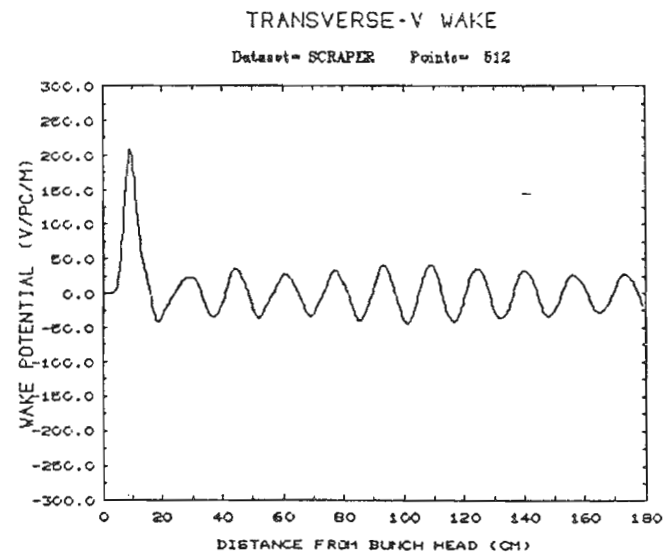
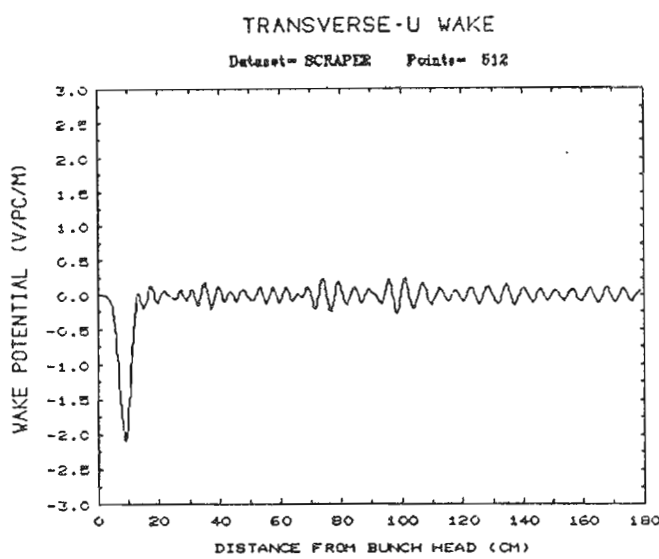
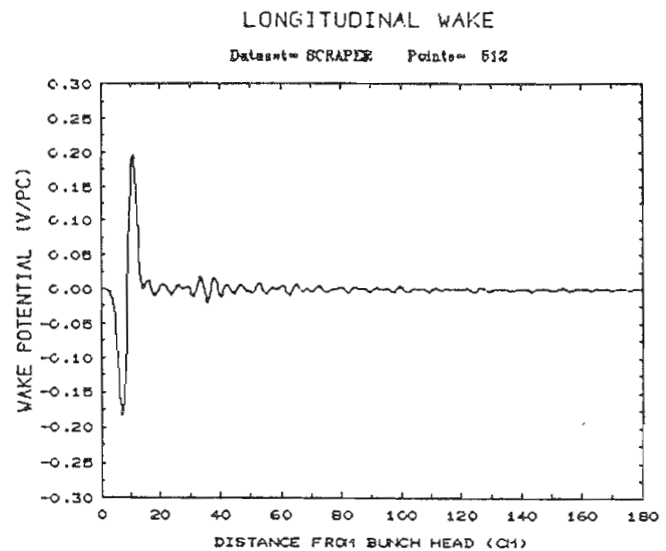
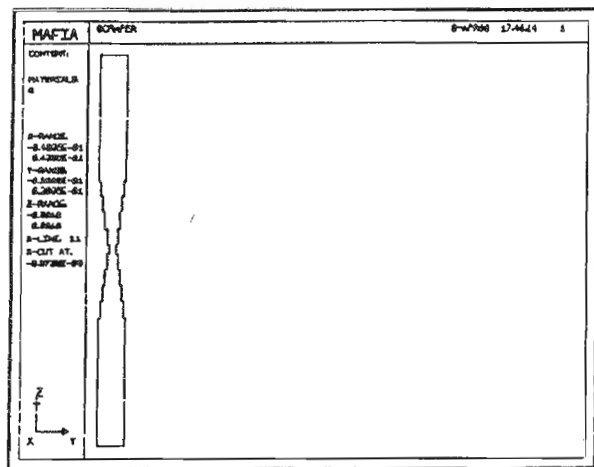
8. THIRD HARMONIC RF CAVITY (1059 MHz).







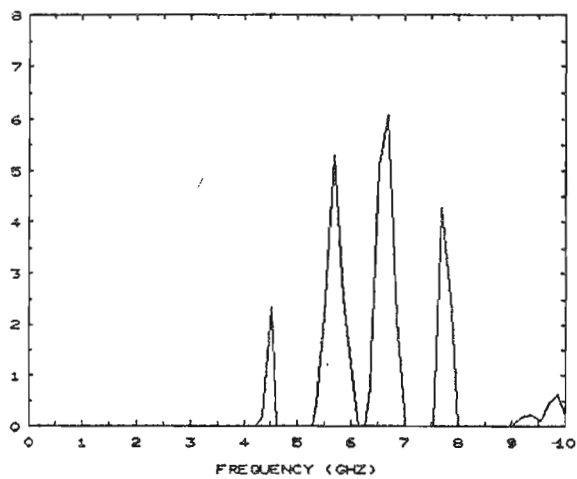
9. BEAM SCRAPER.



REAL LONGI Z (FOR A BUNCH)

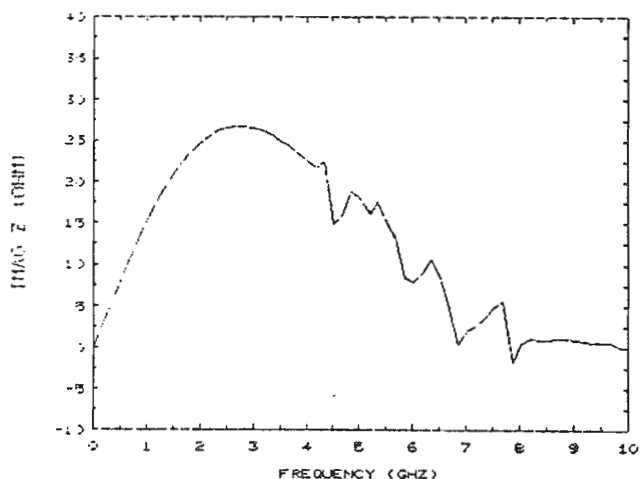
Dataset= SCRAPER Points= 256

REAL Z (OHM)



IMAG LONGI Z (FOR A BUNCH)

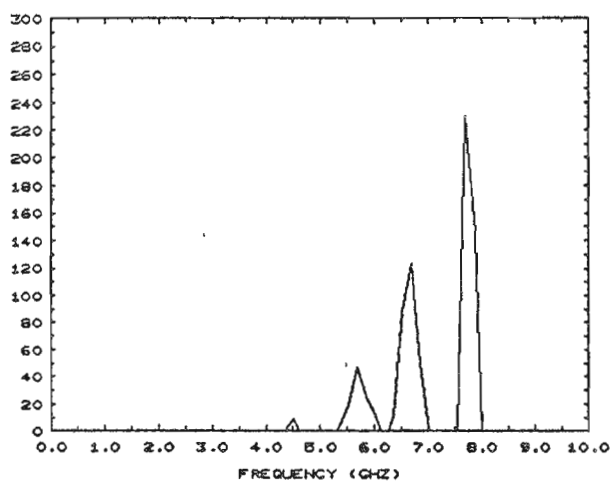
Dataset= SCRAPER Points= 256



REAL LONGI Z (FOR DELTA PASS)

Dataset= SCRAPER Points= 51

REAL Z (OHM)



IMAG LONGI Z (FOR DELTA PASS)

Dataset= SCRAPER Points= 51

